FREQUENCY-DEPENDENT DYNAMICS OF INTRINSIC CONNECTIVITY NETWORKS

by

Hüden Neşe

B.S., in Mathematics, Middle East Technical University, 2010

M.S., in Biomedical Engineering, Boğaziçi University, 2013

Submitted to the Institute of Biomedical Engineering

in partial fulfillment of the requirements

for the degree of

Doctor

of

Philosophy

Boğaziçi University

2024

FREQUENCY-DEPENDENT DYNAMICS OF INTRINSIC CONNECTIVITY NETWORKS

APPROVED BY:

Prof. Dr. Ahmet Ademoğlu .....
(Thesis Advisor)

Prof. Dr. Tamer Demiralp .....
(Thesis Co-advisor)

Prof. Dr. Esin Öztürk Işık .....

Prof. Dr. Burak Güçlü .....

Assoc. Prof. Dr. Koray Çiftçi .....

Asst. Prof. Dr. Ali Bayram .....

DATE OF APPROVAL: 17 December 2024

Dedicated to my migraine, also known as Coşkun, not for being a pain in the neck, but for leading me toward the things that spark my curiosity.

ACKNOWLEDGMENTS

I would like to express my deepest gratitude to everyone who enriched my journey throughout my PhD.

To my advisor, Ahmet Ademoğlu, who gave me the freedom to pursue my research interests, for being so supportive, patient and flexible. You embody the essence of being "kalendermeşrep" more than anyone I have ever known. Beyond the depth of our academic discussions, I was nourished by the coffee breaks in the lab, enriched with conversations about philosophy and history, all accompanied by the aroma of coffee with cardamom.

To my co-advisor, Tamer Demiralp, for being so supportive, inclusive, and meticulous. Thanks to you, I always felt like a true member of HUBAL. Everything I sent you for feedback always came back transformed into a far better version, reflecting your dedication and insight. It was truly inspiring to witness the effort and care you invested in each of your students.

To Hakan Gürvit, for unwittingly teaching me the fundamentals of cognitive neurology. It was only when I began writing my thesis that I fully appreciated how much I had absorbed from you through lab meetings and seminars.

To BME for being such a supportive and friendly community. I am especially grateful to Esin Öztürk Işık for always being there whenever I needed help or encouragement. I also would like to express my heartfelt thanks to Sevgi Öztürk and Morteza Teymoori for providing support and comfort every time I stumbled. The friendships I have formed here have grown into lifelong bonds that extend far beyond academic relationships. To the countless friends and colleagues at BME, you are the heart of what makes this place truly special.

To HUBAL being such a warm and welcoming community. I am especially grateful to Ali Bayram, Emre Harı, and Ulaş Ay for always being available, supportive, and willing to share their time and knowledge.

To Deniz Özen and Burak Kaya for being two unwavering anchors in my life, always present and dependable. We met at times when we knew so little about life, and I am deeply grateful that we navigated and learned everything together.

To my family for being my source of strength, and always standing by my side no matter what. I am lucky to have you!

To Bahadır Topçu for being my lifelong partner, my best friend, my spoon knight, my personal comedian, and so much more. You make life infinitely better! I declare you an honorary doctor :)

This research was supported by funds from TUBITAK ARDEB 1003 Programme (grant number 114E053), Istanbul University Scientific Research Projects Unit (TSA-2022-39128), and Boğaziçi University Scientific Research Funds (grant number 10520) and (grant number 19818).

ACADEMIC ETHICS AND INTEGRITY STATEMENT

I, Hüden Neşe, hereby certify that I am aware of the Academic Ethics and Integrity Policy issued by the Council of Higher Education (YÖK) and I fully acknowledge all the consequences due to its violation by plagiarism or any other way.

Name :

Signature:

Date:

ABSTRACT

FREQUENCY-DEPENDENT DYNAMICS OF INTRINSIC CONNECTIVITY NETWORKS

Despite converging evidence of hierarchical organization in the cerebral cortex, with sensory-motor and association regions at opposite ends, the mechanism of such hierarchical interactions remains elusive. This organization was primarily investigated regarding the spatiotemporal dynamics of intrinsic connectivity networks (ICNs). However, more effort is needed to investigate network dynamics in the frequency domain. We aimed to examine the integrative role of brain regions in the frequency domain with graph metrics. Phase-based connectivity estimation was performed in three frequency bands (0.011-0.038, 0.0433-0.071, and 0.076-0.103 Hz) in the BOLD signal during rest. We applied modularity analysis to connectivity matrices and investigated those areas, which we called integrative regions, that showed frequency-domain flexibility. Integrative regions, mostly belonging to attention networks, were densely connected to higher-order cognitive ICNs in lower frequency bands but to sensory-motor ICNs in higher frequency bands. We compared the normalized participation coefficient values of integrative and core regions with respect to their relation to higher-order cognition using a permutation-based t-test for multiple linear regression. Regression parameters of integrative regions in relation to three cognitive scores in executive functions, and working memory were significantly larger than those of core regions ($P_{fdr} < 0.05$) for salience ventral attention network. Parameters of integrative regions in relation to intelligence scores were significantly larger than those with core regions ($P_{fdr} < 0.05$) in dorsal attention network. Results indicate their essential role at an intermediate level in behavior and emphasize the importance of frequency-band analysis of brain networks.

Keywords: fMRI, Flexibility, Frequency Domain, Integration, Attention Networks.

ÖZET

İÇSEL BAĞLANTISALLIK AĞLARININ FREKANSA ÖZGÜ DİNAMİKLERİ

Duyusal-motor ve ilişkilendirme bölgelerinin beyin korteksinde hiyerarşik bir organizasyona sahip olduğu yönündeki örtüşen kanıtlara rağmen, bu hiyerarşik etkileşimlerin mekanizması hala tam olarak anlaşılamamıştır. Bu organizasyon, genellikle içsel bağlantısallık ağlarının (ICN'ler) mekansal ve zamansal dinamikleri üzerine yapılan çalışmalarla incelenmiştir. Ancak, frekans alanında ağ dinamiklerinin araştırılması konusunda daha fazla çalışmaya ihtiyaç vardır. Bu çalışmada, beyin bölgelerinin frekans alanındaki bütünleştirici rollerini çizge metrikleri kullanarak incelemeyi amaçladık. Dinlenme esnasında BOLD sinyalindeki faza dayalı bağlantısallık üç frekans bandında (0.011-0.038, 0.043-0.071 ve 0.076-0.103 Hz) tahmin edildi. Bağlantısallık matrisleri üzerinde modülerlik analizi yapıldı ve frekans alanı esnekliği gösteren bu bölgeler, entegrasyon bölgeleri olarak adlandırıldı. Bu entegrasyon bölgeleri çoğunlukla dikkat ağlarına ait olup, düşük frekans bantlarında yüksek seviyeli bilişsel ICN'lerle, yüksek frekans bantlarında ise duyusal-motor ICN'lerle yoğun bağlantılar gösterdi. Yüksek düzeyli bilişsel işlevlerle ilişkili olarak, entegrasyon ve çekirdek bölgelerin normalleştirilmiş katılım katsayısı değerlerini permütasyon tabanlı t-testi ile çoklu doğrusal regresyon kullanarak karşılaştırdık. Dikkat çekerlik ventral dikkat ağında, yönetici işlevler ve çalışma belleği gibi üç bilişsel skorla ilişkili olarak entegrasyon bölgelerinin regresyon parametreleri, çekirdek bölgelerinkinden anlamlı derecede daha yüksek çıktı ($P_{fdr} < 0.05$). Dorsal dikkat ağında ise, zeka skorları ile ilişkili olarak, entegrasyon bölgelerinin parametreleri, çekirdek bölgelerinkinden anlamlı derecede daha yüksekti ($P_{fdr} < 0.05$). Sonuçlar bu bölgelerin davranışta ara düzeyde kritik rollerini daha da pekiştirmekte ve beyin ağlarının frekans bandı analizinin önemini vurgulamaktadır.

Anahtar Sözcükler: fMRI, Esneklik, Frekans Alanı, Entegrasyon, Dikkat Ağları.

TABLE OF CONTENTS

ACKNOWLEDGMENTS iv
ACADEMIC ETHICS AND INTEGRITY STATEMENT vi
ABSTRACT vii
ÖZET viii
LIST OF FIGURES xi
LIST OF TABLES xvi
LIST OF SYMBOLS xvii
LIST OF ABBREVIATIONS xviii
1. INTRODUCTION 1
2. BACKGROUND 4
2.1 Brain Dynamics via Functional Neuroimaging 4
2.1.1 Neurovascular Coupling 4
2.1.2 Integration and segregation 4
2.1.3 Brain Networks 7
2.2 Frequency-Dependent Brain Dynamics 17
2.2.1 Time Scales of Brain Activity 17
2.2.2 Time Scales of Resting-State fMRI 19
2.2.3 Temporal Hierarchy in the Cortex 23
2.3 Complex brain networks 24
2.3.1 Connectivity as a Graph 25
2.3.2 Graph metrics on integration and segregation 30
3. MATERIALS AND METHODS 38
3.1 Data 38
3.2 Preprocessing 38
3.3 Connectivity Estimation 41
3.3.1 Identifying the Optimum Sparsity Level 43
3.4 Community Detection and Consensus Clustering 45
3.5 Integrative Regions 49
3.6 Normalized Participation Coefficient 49

3.7 Node Roles of Integrative Regions and Cognition 51
3.8 Statistical Analysis 51
4. RESULTS 54
4.1 Three Main Modules and Corresponding ICNs 54
4.2 Core and Integrative Regions 55
4.3 Core Regions on Attention Networks 56
4.4 Integrative Regions on Attention Networks 56
4.5 Node Roles of Integrative Regions and Cognition 58
5. DISCUSSION 59
5.1 Is the Correlation Coefficient-Based Functional Connectivity Sufficient to Reveal the Network Dynamics? 60
5.2 Can Frequency Characteristics of the BOLD Signal be Significant in Estimating the Network Dynamics? 61
5.3 Intermediate Position of the Two Attention Networks Between the Sensory-Motor and Cognitive Networks 62
5.4 Flexibility of the Attention Networks 62
5.5 Flexible Node-Specific Regression Patterns with Cognitive Test Scores . 63
5.6 Limitations 63
6. CONCLUSION 65
APPENDIX A. PUBLICATIONS 66
REFERENCES 68

LIST OF FIGURES

Figure 2.1	Schematic diagram showing functional segregation and integration [1].	6
Figure 2.2	Representation of the language network from Wernicke's MD thesis [2]. (b) Lichtheim's diagram for the language network [3]. (c) Historical drawing from the original works of Geschwind [4].	8
Figure 2.3	Wernicke-Lichtheim model of language network [5].	8
Figure 2.4	(a) Mesulam's model of spatial attention (1990). (b) Hierarchical organization of brain areas [6]. Unimodal areas: blue and green. Transmodal areas: red.	10
Figure 2.5	Results from the Biswal et al. study [7]. (a) Task-related activation in the motor cortices (b) Functional connectivity during a resting-state scan, with the left motor cortex as the seed region. There is a significant overlap between the task-related and resting-state results.	11
Figure 2.6	Task performance studies have highlighted brain areas (a, top) that reduce activity during tasks (DMN [8]). At rest, these regions (arrows in a, top) display similar signal behavior across areas (a, bottom), a phenomenon first identified by Biswal et al. in the somatomotor cortex [7] and later seen in the DMN. During rest, the brain exhibits anti-correlated networks (b) [9].	12
Figure 2.7	(a) Dorsal and ventral attention networks [10]. (b) Frontoparietal control network (yellow) and cingulo-opercular network (black) [11]. (c) Dorsal attention (green), ventral attention (teal), cingulo-opercular (black), and frontoparietal (yellow) networks [12, 13].	13
Figure 2.8	Intrinsic Connectivity Networks [14].	14
Figure 2.9	Cortical hierarchy defined by (a) Mesulam [6] and (b) Marguiles [15].	16
Figure 2.10	Time scales of brain activity. (a) [16]. (b) [17].	18
Figure 2.11	Oscillatory Signatures in ICNs [18].	20

Figure 2.12 Frequency-specific connectivity maps of (a) visual system and default-mode network (b) amygdala and hippocampus [19]. 21

Figure 2.13 (a) Multilayer framework and (b) structural reducibility method used by De Domenico et al. [20]. 22

Figure 2.14 From Königsberg's seven bridges (a) to Euler's graph (c). The graph is composed of four nodes (A, B, C, D), representing the path of lands, and seven edges, each representing a bridge connecting these regions. (a) From the book Network Science written by Barabasi [21]. (b) From Euler's letter to Carl Leonhard Gottlieb Ehler (1736). (c) From from Euler's paper [22]. 26

Figure 2.15 Parcellation schemas [23]. 27

Figure 2.16 General pipeline for building graph from connectivity [24]. 29

Figure 2.17 Fundamental graph metrics [24]. 30

Figure 2.18 Figurative explanation graph metrics related to segregation and integration [25]. 31

Figure 2.19 The Louvain algorithm for community detection [26]. 33

Figure 2.20 Consensus clustering algorithm [27, 28]. Two partitions with approximately the same quality ($Q = 0.54$) might show different community assignments. 34

Figure 2.21 Flexibility [29]. 36

Figure 3.1 Schaefer's parcellation (400 parsel, 7 network) [30]. 39

Figure 3.2 Workflow overview. First, we calculated phase consistency matrices and thresholded them. Then, we performed a modularity analysis followed by twofold consensus clustering to determine the subject-level modular organization and a third-fold one to identify the group-level modules. We utilized the results of the group-level modular organization to define the flexible regions over frequency bands. We examined the connector role of brain regions in the network by calculating the normalized participation coefficient for each parcel using subject-level information. Finally, we studied the relation of these node-specific graph metric values of integrative and core regions to high-order cognition. 40

Figure 3.3 Phase differences between parcel pairs were calculated for each time window and frequency bin (a), these phase difference matrices were used to compute phase consistency for three frequency bands (b). PC, Phase Consistency; Fb1, 0.011-0.038Hz; Fb2, 0.043 - 0.071Hz; Fb3, 0.076 - 0.103Hz. 42

Figure 3.4 Connectivity matrices were thresholded at different sparsity levels (from 0.05 to 0.40 with 0.01 intervals) for each frequency band and each subject (a). Each thresholded matrix was used to generate 100 randomized networks (b). Randomized networks were used to calculate the small-worldness index (c). Percolation analysis was applied to the mean thresholded connectivity matrix to identify the sparsity level at which the largest connected component started breaking apart (d). $P = 400$ (parcels); $S = 96$ (subjects); $F = 3$ (frequency bands); $T = 5$ (proportional thresholds); $R = 100$ (randomizations). 44

Figure 3.5 Therefore, using percolation analysis, we identified the optimum sparsification threshold as 30% and applied it to PC networks in further analysis. 45

Figure 3.6 Consensus Clustering algorithm [27, 28]. 46

Figure 3.7 Similarity between Schaefer's parcels assigned to seven networks and the subject-level modular organization at each γ value. Shaded areas indicate the standard deviation of the mean over subjects. z-Rand has its maximum values in a range from 1 to 1.9. 48

Figure 3.8 Connectivity matrices were thresholded at a sparsity level of 30% for each frequency band and each subject (a). Each thresholded matrix was randomized 100 times to generate null networks (b). The modularity algorithm using various γ values was applied 100 times to each $P \times P$ matrix to obtain Q values (c1). The modularity algorithm was applied to each $P \times P$ matrix using various γ values to obtain Q_{rand} values (c2). To test the difference between Q and Q_{rand} over subjects, we took the average over iterations for Q and randomizations for Q_{rand}. $P = 400$ (parcels); $S = 96$ (subjects); $F = 3$ (frequency bands); $R = 100$ (randomizations); $G = 29$ (γ values); $I = 100$ (iterations). 48

Figure 3.9 Flexibile and core regions. 49

Figure 3.10 Figurative explanation of participation coefficient. 50

Figure 4.1 We performed a one-sample t-test over subjects to determine whether that difference was significantly greater than or less than zero for each γ value. Boxplots show the modularity index Q in the brain network compared to randomized networks (Q_{rand}). Error bars indicate the standard deviation in the mean over subjects. *** indicates that $p_{\text{fdr}} < 0.001$ for the one-sample t-test where p_{fdr} stands for the FDR-corrected p-value. 54

Figure 4.2 Three main modules were revealed via group-level analysis. Module 1 covers the VN and parts of the DAN, Module 2 covers the DMN, ECN, and LN, and Module 3 contains the SMN and parts of the SN/VAN. Dots identify the module assignment of each parcel. Parcels belonging to attention networks are distributed among these three modules. Shaded areas correspond to attention networks (a). Core parcels assigned to the same module in all three frequency bands are represented on the cortex (VN, visual network; DAN, dorsal attention network; DMN, default mode network; ECN, executive control network; LN, limbic network; SMN, somatomotor network; SN/VAN, salience/ventral attention network) (b). 55

Figure 4.3 Core Regions on Attention Networks. 56

Figure 4.4 Core and integrative regions within the attention networks. White parcels are the integrative regions, while core regions are color-coded. Module1, Module2, and Module3 are dominated by VN, DMN, and SMN, respectively. VN, visual network; DMN, default mode network; SMN, somatomotor network. 56

Figure 4.5 Frequency selective module participation of integrative regions in attention networks. Integrative regions participate in the cognitive module at a frequency band and in either one of the visual or somatomotor modules in another frequency band. Yellow indicates the core parcels. Modular assignments of integrative regions in different frequency bands were color-coded. Module1, CN-centred; Module2, Cognitive; Module3, SMN-centred. VN, visual network; DMN, default mode network; SMN, somatomotor network; TPJ, temporoparietal junction; AI, anterior insula; ACC, anterior cingulate cortex; FEF, frontal eye field; IFJ, inferior frontal junction. 57

Figure 5.1 Flexible nodes with connector role. 63

LIST OF TABLES

Table 3.1 Behavioral data for fluid intelligence and five cognitive domains of interest (two test scores for each domain). 51

Table 4.1 Significant results of permutation-based t-tests showed that the P^{norm} of integrative regions differed from the core regions regarding their relation with high-order cognition such as intelligence, executive functions, and working memory. 58

LIST OF SYMBOLS

S	Number of subjects
F	Number of frequency bands
I	Number of iterations
R	Number of randomizations
T	Number of proportional thresholds
$Fb1, Fb2, Fb3$	Three frequency bands
a_{ij}	Entry in the adjacency matrix representing the presence of an edge
w_{ij}	Weight of the edge connecting node i and j
W	Total weight of edges in the network
$\delta(m_i, m_j)$	Kronecker delta
γ	Resolution parameter
M	Partition
Q	Modularity index
Q_{rand}	Modularity index of randomized network
PC^{norm}	Normalized participation coefficient
$flex_i$	Flexibility of parcel i
σ	Small-Worldness Index
c	Contrast vector
Y	Behavioral data
X	Design matrix
β	Linear regression parameters
$\hat{\beta}$	Estimated regression parameters
$\hat{\sigma}^2$	Standard deviation of the residual error
ϵ	Error
I	Identity matrix
R	Residual matrix

LIST OF ABBREVIATIONS

ACC	Anterior Cingulate Cortex
AI	Anterior Insula
ALFF	Amplitude of Low-Frequency Fluctuations
BOLD	Blood-Oxygen-Level Dependent signal
CC	Correlation Coefficient
CSF	Cerebrospinal Fluid
DAN	Dorsal Attention Network
DCCS	Dimensional Change Card Sort
DLPFC	Dorsolateral Prefrontal Cortex
dFC	Dynamic Functional Connectivity
DMN	Default Mode Network
DTI	Diffusion Tensor Imaging
ECoG	Electrocorticography
ECN	Executive Control Network
EEG	Electroencephalogram
FEF	Frontal Eye Field
FD	Framewise Displacement
FDR	False Discovery Rate
FC	Functional Connectivity
GLM	General Linear Modeling
GM	Gray Matter
GSR	Global Signal Regression
HCP	Human Connectome Project
ICA	Independent Component Analysis
ICN	Intrinsic Connectivity Networks
IFJ	Inferior Frontal Junction
IPS	Intraparietal Sulcus
LFP	Local Field Potential

LN	Limbic Network
mPFC	Medial Prefrontal Cortex
MEG	Magnetoencephalography
MRI	Magnetic Resonance Imaging
PC	Phase Consistency
PCC	Posterior Cingulate Cortex
PMAT	Penn Progressive Matrices
ReHo	Regional Homogeneity
SMN	Somatomotor Network
SN/VAN	Salience Ventral Attention Network
TE	Echo Time
TNN	Task-Negative Network
TPJ	Temporoparietal Junction
TPN	Task-Positive Network
TR	Repetition Time
VAN	Ventral Attention Network
VN	Visual Network
WM	White Matter
z-Rand	z-score of the Rand Similarity Coefficient

1. INTRODUCTION

The brain is a complex system that generates an extensive repertoire of cognitive and behavioral states by blending integration and segregation processes [31]. Different functional domains are assumed to be represented in large-scale networks called resting-state (RSNs) or intrinsic connectivity networks (ICNs). Generally, these networks can be observed as stationary functional connectivity (FC) patterns within the low-frequency portion of the functional magnetic resonance imaging (fMRI) signal ranging from 0.01 Hz to 0.1 Hz [32]. Visual (VN), somatomotor (SMN), dorsal attention (DAN), salience/ventral attention (SN/VAN), limbic (LN), executive control (ECN), and default mode networks (DMN) are the commonly acknowledged ICNs [33]. There is converging evidence for the existence of a hierarchical organization in the cerebral cortex, with sensory-motor and supervisory heteromodal association regions at the opposite ends of the hierarchy [6]. Margulies et al. proposed an overarching organization of ICNs in which the default-mode network (DMN) is situated at the top of a representational hierarchy, while the intermediate zone is occupied by attention networks and the bottom range consists of sensory-motor networks [15]. The mechanisms of how these three major hierarchical layers interact with each other to strike a balance between integration and segregation still remain elusive.

Graph Theory provides practical tools like community detection that helps us to investigate segregational and integrative features of the brain organization [26]. Numerous studies using community detection algorithms on structural and functional brain networks reported compelling evidence of the modular structure of brain connectivity [34]. Guimera and Amaral have proposed two graph metrics namely, the within-module degree z-score and the participation coefficient (P), to characterize how the connections of a node were distributed within and between modules [35]. Nodes with higher participation coefficients are considered as connectors due to their various intermodular connections and it is assumed that they support costly and integrated activity required for effortful, domain-general cognitive processes [26].

While the conventional FC literature is primarily dedicated to characterizing long-lasting patterns of integrative/segregative organization in the brain, many research groups focused on the dynamic FC (dFC) in order to study the time-varying interactions among the ICNs [36]. One of the important consequences of dFC studies is the discovery of another valuable graph metric called flexibility [37] which is used to express the extent to which a node can exhibit variability in associating itself with different modules in different time windows [38]. However, no previous study investigated the flexibility of a node in terms of its simultaneous association with different modules in different frequency ranges. This property might explain more efficiently the integrative role of a flexible node in binding the processes running in different ICNs or modules.

In contrast to fMRI literature, the electrophysiological studies based on electroencephalogram (EEG) or magnetoencephalogram (MEG), which provide high temporal resolution and a wider frequency range, have been extensively studied in the frequency domain in order to delineate the temporal superimposition of different neuronal circuits that operate in different frequency ranges [39]. Additionally, it has been argued that generally the higher frequencies in the gamma frequency range are associated with earlier sensory or motor processing in local circuits, while multimodal integration among neighboring areas is mainly associated with the beta band at a slightly lower frequency range. However, long-range interactions in the fronto-parietal circuits evolved in the lower frequency ranges of alpha and theta oscillations [40]. Furthermore, it has been shown that parallel operating circuits in different frequency bands interact by means of cross-frequency couplings [41] whose patterns may explain part of the BOLD amplitude variation [42]. While these studies provided valuable information about the integration within and among parallel processing circuits in the brain, the poor spatial resolution of the electrophysiological signals did not permit a precise description of the neuroanatomical counterparts. We propose that this gap can be filled with fMRI-based flexibility analysis in the frequency domain if different frequency bands in the BOLD signal would correspond to participations with different modules as they have already been shown for the electrophysiological signals. The evidence for different patterns of FC [19,43], as well as regional homogeneity (ReHo) [44] and power [45] among different

frequency bands of the BOLD signal, constitute clues in this direction.

Inspired by these works, we propose that the decomposition of the conventional BOLD frequency band into sub-bands may allow for the observation of simultaneous, parallel processes, which can provide a mechanistic perspective on the integration among modular structures. Considering the low temporal resolution of the fMRI signal, we aim in this stage to search for frequency-selective stationary patterns for such an integration. Similar to temporal flexibility in dFC studies, we need to refer to a concept called frequency-domain flexibility, which corresponds to different modular associations of the same node in different frequency bands. We hypothesize that the flexible/integrative areas are simultaneously recruited by different communities in different frequencies, while other nodes correspond to the core regions of each module. In order to test this hypothesis, we also compared the flexible and core module regions in terms of the correlations between their graph metrics (z and P) and the neuropsychological test scores of the subjects. This study aims to investigate the integrative role of brain regions with the help of graph theory. Based on the above considerations, we hypothesize that the flexible/integrative brain areas are simultaneously recruited by different communities manifested as different modular associations in different frequency bands in the BOLD signal, while core regions preserve their modular participation across frequency bands. Considering such a proposed hierarchical organization among ICNs, we expect flexible areas to lie primarily in attention networks that bridge the two ends of the hierarchy.

2. BACKGROUND

2.1 Brain Dynamics via Functional Neuroimaging

2.1.1 Neurovascular Coupling

Oscillatory dynamics of neural activity can be assessed at various scales, such as local field potential (LFP), electrocorticography (ECoG), and electroencephalography (EEG) signals. Each of these signals reflects the summed electrical activity in the brain, which manifests as neural oscillations. Beyond electrophysiological techniques, functional brain imaging methods like fMRI provide an alternative view of brain function. While EEG measures the electrical dimension of neural activity via electrodes placed on the scalp, fMRI allows for the measurement of changes in the ratio of oxyhemoglobin to deoxyhemoglobin in the brain, which is a result of vascular responses [46]. Unlike EEG, which directly captures neural activity, fMRI provides an indirect measurement by analyzing changes in blood volume, oxygenation, and flow. When a specific brain region becomes more active, it requires more energy, which increases the demand for ATP. This demand for energy leads to a sudden increase in blood flow to the active area, supplying more oxygen. As more oxygenated blood arrives, the oxyhemoglobin level rises, and the deoxyhemoglobin level falls. This shift in oxygen levels produces a measurable signal known as the BOLD (Blood oxygen level dependent) response. Since deoxyhemoglobin is paramagnetic (affects magnetic signals), its reduction enhances the MRI signal by about 2-4 %. fMRI uses these changes in the MRI signal to map active regions of the brain, providing valuable insights into brain function [46–48].

2.1.2 Integration and segregation

Throughout the history of neuroscience, one of the most important questions has been understanding the neural mechanisms underlying sensory and cognitive processes.

While it is now widely accepted that the brain regulates information flow through a balance of segregated and integrated activity, early theories like localizationism suggested that distinct brain regions, rather than the whole brain, are responsible for specific functions [49].

Localizationism was initially inspired by Franz Joseph Gall's theory of phrenology, which lacked a rigorous experimental foundation. However, in the 19th century, Pierre Broca and Karl Wernicke made significant contributions to functional localization in the brain using detailed studies of patients with brain injuries [50]. With the rise of functional brain imaging techniques like fMRI, localizationism experienced a revival since these methods were able to demonstrate that specific brain regions were active during certain experimental conditions. The first two decades of fMRI research mainly focused on identifying anatomical changes in the BOLD signal using linear models [51]. However, it has become increasingly evident that even the simplest sensory processes are supported by various brain regions [52]. As a result, researchers have shifted their attention toward understanding the interactions among multiple brain regions, which is called functional integration. Therefore, the idea of mapping functions to individual brain areas became outdated [53].

Functional integration was proposed by Flourens in 1824 as a challenge to localization theory. It does not contradict the idea of functional segregation but mainly complements it by highlighting the importance of interaction between segregated brain regions. One of the main tools for analyzing distributed brain processing is estimating functional connectivity from signals obtained from different brain areas [54–56]. Functional connectivity is the statistical relationship between distant neurophysiological events, typically measured as simple correlation or coherence analyses of fMRI or electrophysiological time series. Although functional connectivity studies have offered valuable insights into how brain regions interact, understanding the underlying mechanisms of distributed processing remains a fundamental challenge in neuroscience.

In recent years, network-based models of brain activity have been recognized for their value, as they provide valuable insights into neuronal communication across

brain regions [57]. These networks are represented as graphs consisting of nodes (brain regions) and edges (connections or pathways). Then, they can be examined using a variety of quantitative tools [1,24]. Large-scale brain connectivity has been studied via graph theory/network analysis to reveal the key features that promote the segregation and integration of neural information, primarily through two attributes: communities and hubs (Figure 2.1). Communities are groups of regions that are highly interconnected, with fewer connections between different communities. This structure supports functional specialization in the brain. Hubs act as bridges between different communities, ensuring the integration of information across the brain.

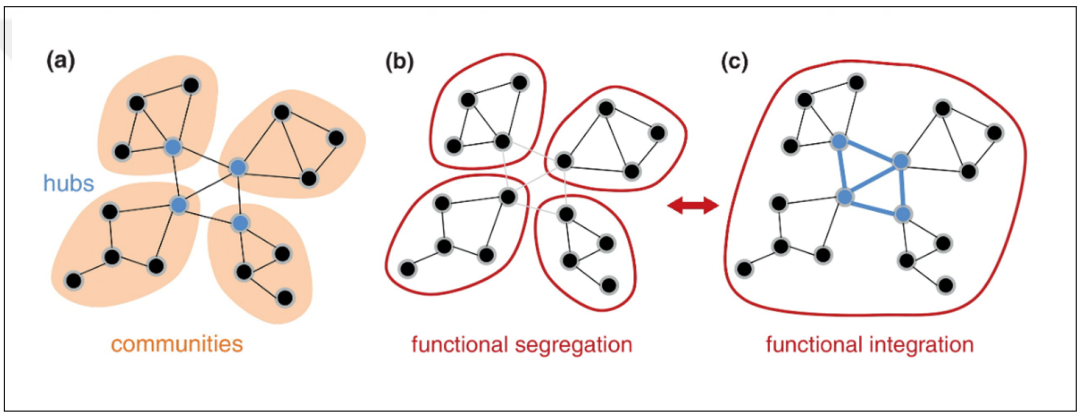

Figure 2.1 Schematic diagram showing functional segregation and integration [1].

The brain's functional organization is dynamically reconfigured to support a wide range of cognitive tasks [58, 59]. Research has shown that different cognitive tasks require varying segregation and integration of distributed brain regions [1, 60]. For example, simple motor tasks are associated with higher segregation, while tasks requiring more cognitive effort tend to involve greater integration [31, 61].

Network-based models also highlighted the significance of brain network segregation and integration and their relation to behavior. The brain's functional organization at rest can reflect task-related activity patterns, allowing it to predict task performance such as general intelligence [62], working memory capacity [63], and other cognitive functions (Kelly et al., 2008; Mennes et al., 2011).

Research suggests that healthy resting brains function near a critical state, allowing for exploration and switching among the different brain states, supporting

various cognitive functions [60, 64, 65]. Consequently, resting brains are thought to maintain a balance between segregation and integration to meet varying cognitive demands [66,67]. Recent advancements in methods for studying the time-varying properties of fMRI functional connectivity have provided valuable insights into the temporal dynamics of network integration and segregation [36, 68–70]. However, the frequency domain dynamics of these processes have not yet been explored in depth, leaving an important gap in our understanding of brain network dynamics.

2.1.3 Brain Networks

2.1.3.1 First brain network

The earliest attempts to reveal large-scale interconnected cortical areas are network diagrams drawn by clinicians like Theodor Meynert, Carl Wernicke, and Ludwig Lichtheim [26]. Their objective was to map the white matter pathways connecting different brain regions and show how the symptoms of brain disorders could be connected to lesions. In the 19th century, French neurosurgeon Paul Broca and German neurologist Carl Wernicke identified specific brain regions that damage to these regions led to distinct language disorders. Broca's area, located in the left posterior inferior frontal gyrus, is responsible for speech production [71]. A lesion in this area leads to difficulties in forming speech (Broca's aphasia), while comprehension remains mostly preserved. Wernicke's area, situated in the left posterior superior temporal gyrus, plays a crucial role in language comprehension [2]. Wernicke's aphasia occurs due to damage in this area, leading to impaired language comprehension while speech production remains fluent.

In 1874, Wernicke elaborated the first network model of language, suggesting that disconnection between these two cortical regions could result in difficulties with word repetition, a condition he termed 'conduction aphasia' (Figure 2.2, a). In 1885, Lichtheim not only sketched Wernicke's ideas into a diagram but also extended the model by introducing additional association areas. In his diagram, A refers to an

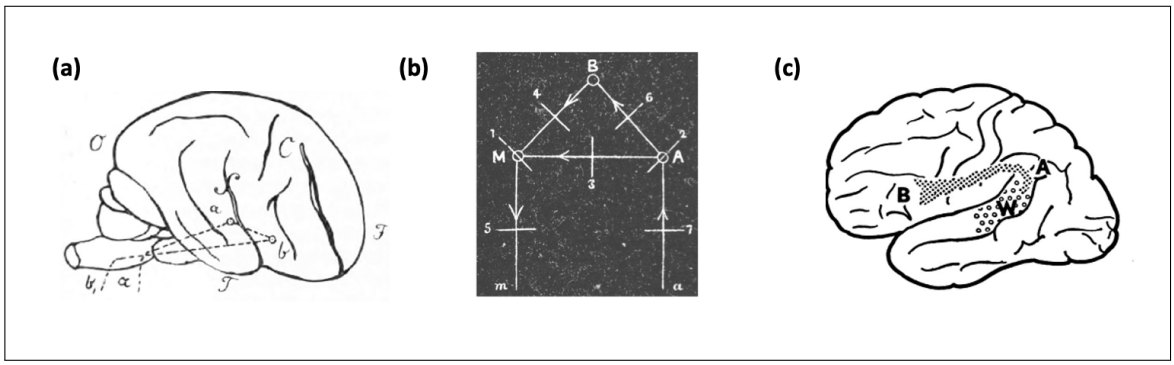

Figure 2.2 Representation of the language network from Wernicke's MD thesis [2]. (b) Lichtheim's diagram for the language network [3]. (c) Historical drawing from the original works of Geschwind [4].

auditory region (Wernicke's area), M represents a motor region (Broca's area), and B denotes other association areas (Figure 2.2, b). Although we now know the modern language network model is significantly more complex than the Wernicke-Lichtheim language model (Figure 2.3), it is considered one of the most successful early models of brain network organization.

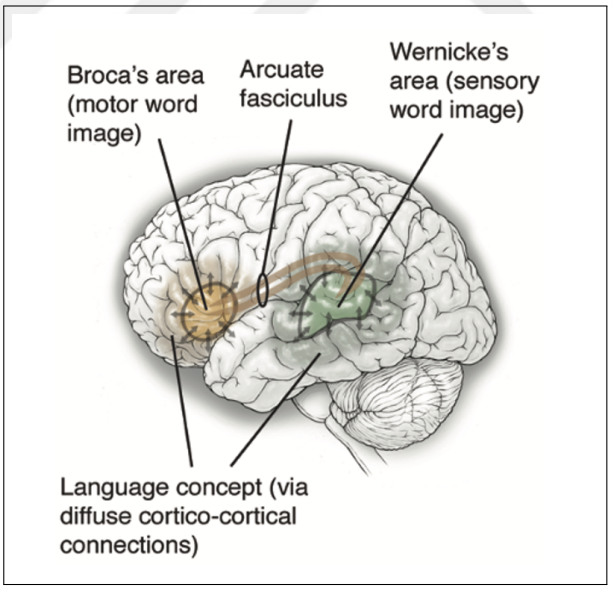

Figure 2.3 Wernicke-Lichtheim model of language network [5].

Despite initial skepticism of the Wernicke-Lichtheim model, Norman Geschwind later strengthened the "disconnection hypothesis" by proposing that conduction aphasia was caused by lesions in the arcuate fasciculus, a white matter tract connecting the Broca's area to Wernicke's area [4]. He also expanded the concept of disconnection syndromes to include not only white matter lesions but also damage to the associa-

tion cortex. These studies sparked interest in cognitive models based on large-scale distributed networks [72].

2.1.3.2 Modern Discovery of Brain Networks

From Sensation to Cognition

In 2015, Marcel Mesulam wrote an article titled "Fifty Years of Disconnexion Syndromes and the Geschwind Legacy" to honor Norman Geschwind's contributions [73, 74]. The article opens with a quote from Orhan Pamuk's Yeni Hayat: "I read a book one day and my whole life was changed... I sat at the table turning the pages, my mind barely aware that I was reading, and my whole life was changing as I read the new words on each page." Mesulam adds, "Had Pamuk's protagonist been a behavioral neurologist, he might have chosen similar words to describe his first encounter with Norman Geschwind's 1965 Disconnexion Syndromes in Animals and Man. His experience would not have been unique. For the past half-century, this two-part monograph has remained the most influential work ever published in the discipline that came to be known as behavioral neurology." Geschwind's ideas not only influenced neurologists like Marsel Mesulam and Antonio Damasio, who further developed and refined his model, but they also redirected the focus from localized brain damage to a broader, connectionist perspective of brain functionality. This shift played a pivotal role in the subsequent emergence of network neuroscience. Geschwind suggested that certain neurological disorders, particularly those affecting higher cognitive functions, can result from the loss of communication between brain areas. In 1998, Mesulam expanded on Geschwind's framework, highlighting the importance of large-scale neurocognitive networks and hierarchical processing in cognitive functions (Figure 2.4) [6]. He articulated that the human brain is composed of at least five core functional networks: (i) the spatial attention network, (ii) the language network, (iii) the explicit memory network, (iv) the face-object recognition network, and (v) the working memory-executive function network. He identified primary, unimodal association, and heteromodal association cortices as part of a hierarchical system and claimed that neurocognitive networks con-

sist of these areas. He also suggested that higher cognitive functions, such as attention, memory, language, and executive control, emerge through interactions between these networks.

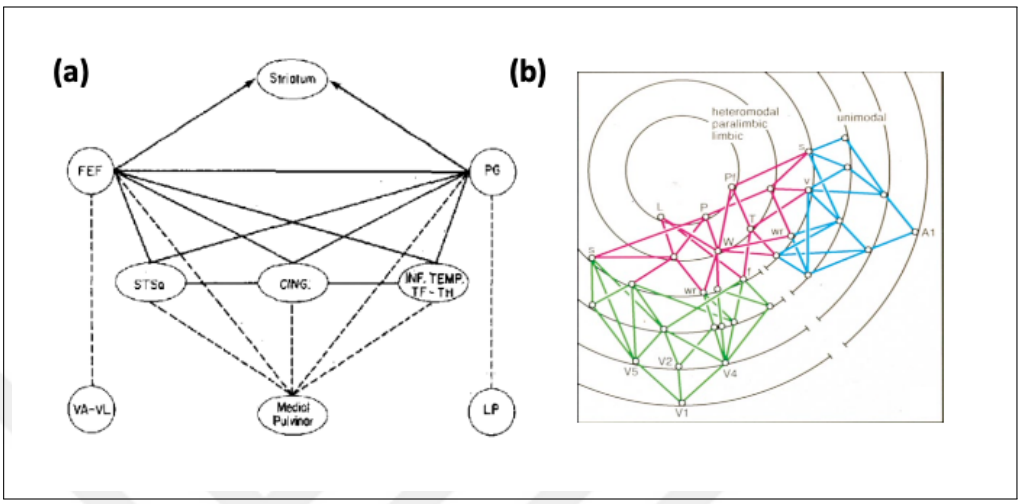

Figure 2.4 (a) Mesulam's model of spatial attention (1990). (b) Hierarchical organization of brain areas [6]. Unimodal areas: blue and green. Transmodal areas: red.

Mesulam's framework was initially based on clinical observations and lesion studies. With the progress of functional neuroimaging techniques, neuroscientists have been able to map brain networks in more detail. The development of Intrinsic Connectivity Networks (ICNs) expands on Mesulam's ideas, highlighting the brain's ability to maintain spontaneous activity even during rest.

Intrinsic Connectivity Networks

Early studies demonstrated that resting-state activity is not random, but rather organized into coherent patterns across various brain networks. Biswal et al. [7, 75] discovered that the motor cortex in both hemispheres exhibits high correlations during rest, similar to those seen during active motor tasks (Figure 2.5). This suggested that the brain's resting-state activity preserves essential functional connectivity patterns for sensory and motor processing, even when no external stimuli are present [7, 76]. These findings challenged the prior belief that resting-state BOLD activity was just noise. Later studies replicated these results in other networks, including visual, auditory, and higher-level cognitive networks [32, 77–79].

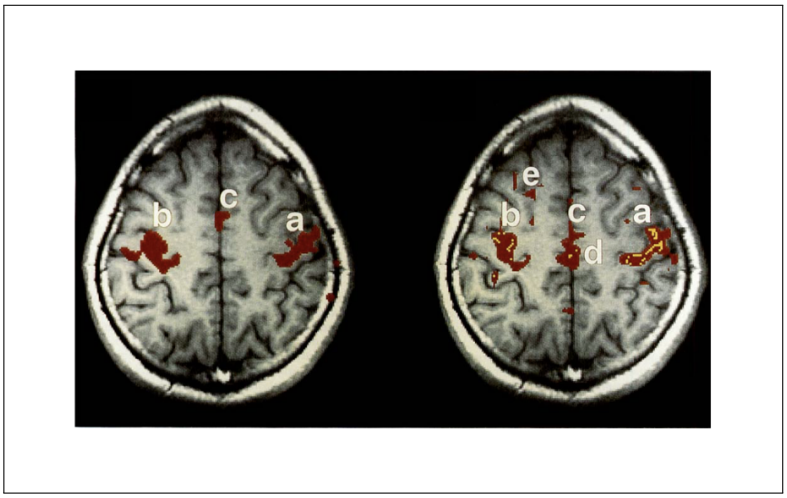

Figure 2.5 Results from the Biswal et al. study [7]. (a) Task-related activation in the motor cortices (b) Functional connectivity during a resting-state scan, with the left motor cortex as the seed region. There is a significant overlap between the task-related and resting-state results.

Shulman et al. [80] were the first to show that certain brain regions deactivate during goal-oriented tasks, providing the basis for the discovery of the default mode network (DMN). Their PET scans consistently revealed that areas such as the posterior cingulate cortex and medial prefrontal cortex exhibited task-induced deactivations, indicating a baseline state of brain activity. Building on these findings, Raichle and colleagues [8] formally identified the DMN, which includes key areas like the medial prefrontal cortex, posterior cingulate cortex, and angular gyrus. These regions show reduced activity during tasks that require external attention but become more active during rest. Buckner et al. [81] expanded this understanding by integrating PET meta-analyses with fMRI data to explore the DMN's role in memory retrieval, further emphasizing its significance in the brain's intrinsic connectivity. The study emphasized the DMN's involvement in internal cognitive processes and its potential connection to neurological and psychiatric disorders, including Alzheimer's disease.

In 2005, Fox and colleagues identified two major networks in the brain that operate in opposing ways during task performance: the task-positive network (TPN), responsible for externally directed, goal-oriented attention, and the task-negative network (TNN), which governs internally-directed thought during rest (Figure 2.6) [9]. The task-positive network includes regions such as the dorsolateral prefrontal cortex (DLPFC), intraparietal sulcus (IPS), and frontal eye fields (FEF), which are involved

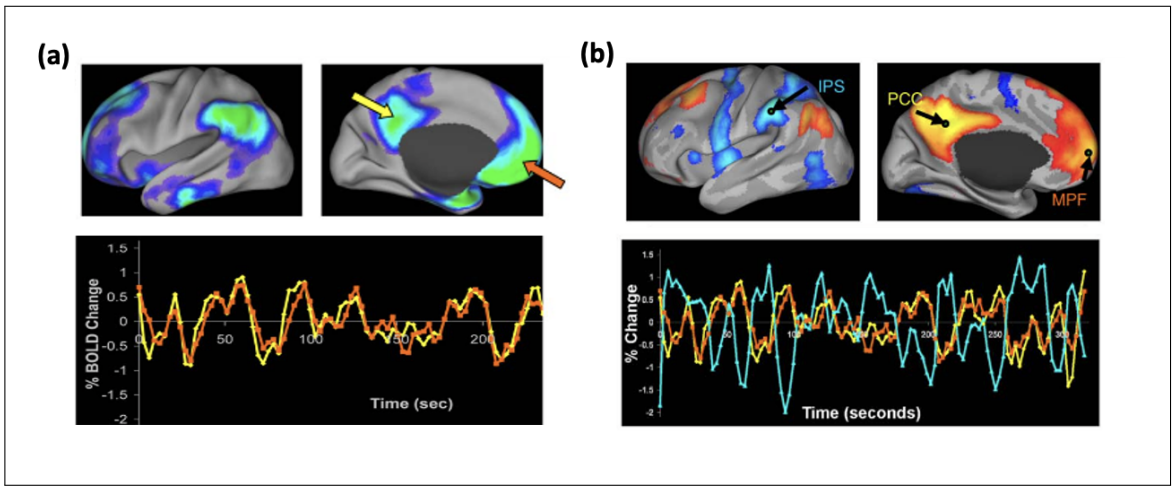

Figure 2.6 Task performance studies have highlighted brain areas (a, top) that reduce activity during tasks (DMN [8]). At rest, these regions (arrows in a, top) display similar signal behavior across areas (a, bottom), a phenomenon first identified by Biswal et al. in the somatomotor cortex [7] and later seen in the DMN. During rest, the brain exhibits anti-correlated networks (b) [9].

in attention, working memory, and executive control. The task-negative network, often synonymous with the DMN, includes regions like the medial prefrontal cortex (mPFC), posterior cingulate cortex (PCC), and precuneus, which are involved in self-referential thoughts, mind-wandering, and autobiographical memory.

Long before the discovery of the default mode network, Peterson and Posner proposed that the attention system is composed of three distinct, anatomically separate networks: alerting, orienting, and executive control (Figure 2.7) [82]. During the 2000s, methodological advancements allowed for a more detailed investigation of these networks. Functional connectivity methods, such as independent component analysis (ICA) and seed-based correlation analysis, were refined to better identify consistent patterns of activity across participants [83]. Corbetta and Shulman [10] introduced two distinct attention networks: the dorsal frontoparietal network for voluntary, top-down attention and the ventral frontoparietal network for detecting unexpected stimuli and shifting attention. Later, Dosenbach et al. [84] identified two executive control networks: the frontoparietal control network, involved in task initiation and error correction, and the cingulo-opercular control network, which sustains attention and task performance throughout execution. Additionally, Seeley et al. [85] identified the salience network within the cingulo-opercular regions, highlighting its role in detecting

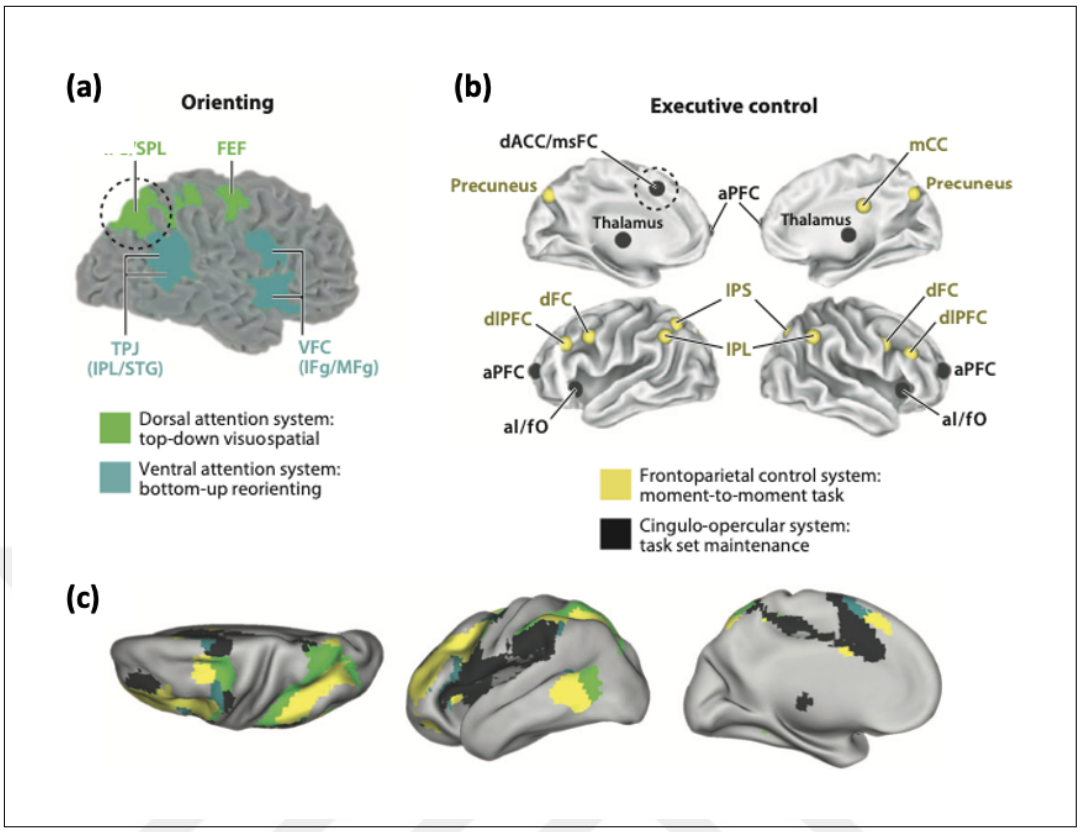

Figure 2.7 (a) Dorsal and ventral attention networks [10]. (b) Frontoparietal control network (yellow) and cingulo-opercular network (black) [11]. (c) Dorsal attention (green), ventral attention (teal), cingulo-opercular (black), and frontoparietal (yellow) networks [12, 13].

emotionally significant stimuli and linking to the brain's reward system.

Determining the exact number of functional brain networks is challenging due to the brain's hierarchical organization [86]. Techniques, such as ICA, clustering, and meta-analysis have identified various number of networks from 5 to 17 [33, 77, 87], with different naming conventions. Both coarse and fine-grained analyses can offer valid insights into how brain networks function. Nonetheless, based on previous studies [33, 83, 88], a core framework of six ICNs can be considered a fundamental foundation for understanding brain organization (Figure 2.8):

Visual Network (VN): This network is mainly responsible for visual information processing. Its core regions are located in the occipital lobe, including the primary visual cortex (V1) and surrounding areas that handle more complex aspects of visual perception [83].

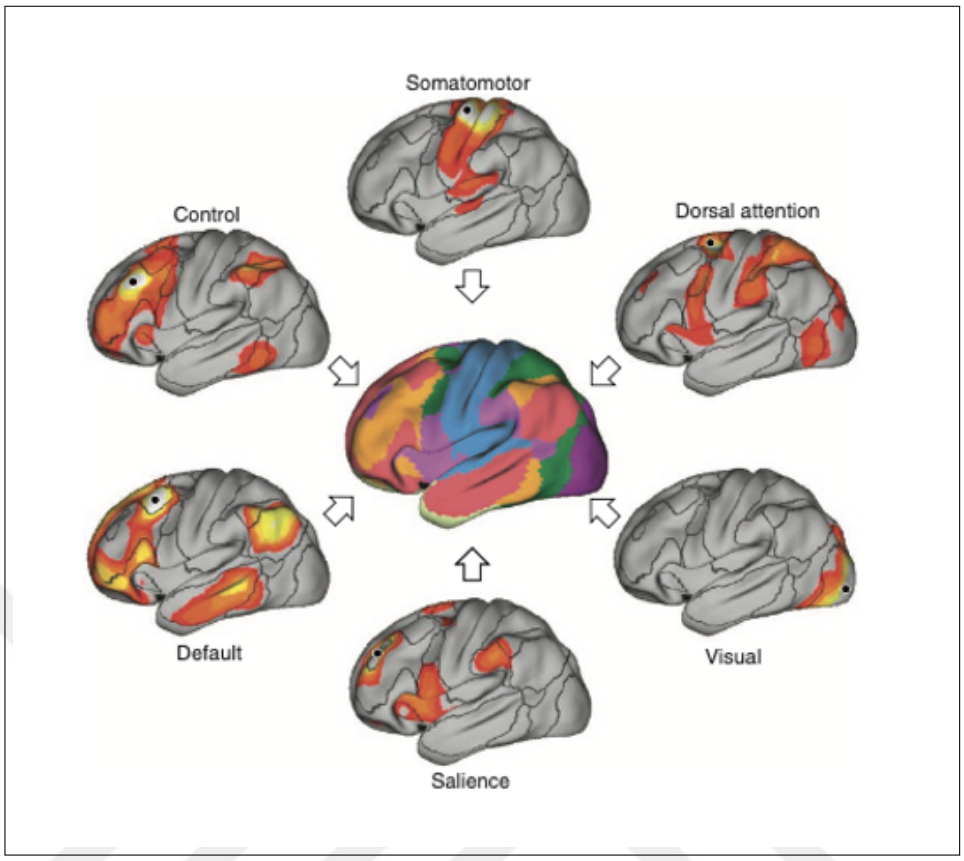

Figure 2.8 Intrinsic Connectivity Networks [14].

Somatomotor Network (SN): This network plays a key role in motor control and somatosensory processing. Its core regions are situated around the motor and somatosensory cortices on both sides of the central sulcus, with additional involvement from the supplementary motor area and occasionally the auditory cortex [83].

Dorsal Attention Network (DAN): It is responsible for top-down, goal-directed attention and visuospatial processing. Its core regions include the superior parietal lobule, intraparietal sulcus, middle temporal complex, and frontal eye fields, with additional areas like the ventral premotor cortex and dorsolateral prefrontal cortex contributing to its functions [83]. DAN handles goal-directed, voluntary attention; recent findings highlight the involvement of the inferior frontal junction (IFJ) and its dynamic connectivity with different brain areas during both voluntary and stimulus-driven attention [89].

Salience Ventral Attention Network (SN/VAN): The boundaries between

the salience network, ventral attention network, and cingulo-opercular network are still under debate [33, 90]. Here, we adopt Yeo's definition for clarity. This network is a crucial brain system for detecting and responding to important stimuli, both from the environment and within the body or mind. Core regions include the anterior insula and midcingulate cortex, with additional involvement from regions like the inferior parietal cortex, temporal parietal junction, and lateral prefrontal cortex [83]. This network is crucial for detecting important stimuli and coordinating neural resources. It acts as a switch between the DMN and executive control network (ECN), managing transitions between rest and goal-directed tasks [91]. Therefore, it plays a vital role in attention, emotional regulation, and shifting focus between internal and external states, influencing cognitive, emotional, and social processes, including empathy and decision-making [92].

Executive Control Network (ECN): This network is essential for executive functions such as goal-directed behavior, working memory, task switching, and inhibition. It consists of regions in the lateral prefrontal cortex, anterior inferior parietal lobule, and midcingulate gyrus with additional areas like dorsal precuneus and posterior inferior temporal lobe [83]. ECN interacts with both internal and external cognitive systems and has subsystems that connect to different networks, supporting either internally or externally directed cognitive processes [93, 94].

Default Mode Network (DMN): This network is essential for internally focused cognitive tasks like self-reflection, imagination, memory retrieval, and social cognition. It involves key brain regions such as the medial prefrontal cortex, posterior cingulate cortex, and inferior parietal lobule. While originally considered a task-negative network, more recent research highlights its involvement in cognitive processes, including goal-directed tasks [95].

Moreover, ICNs are not limited to fMRI; they have been identified using other modalities, including arterial spin labeling perfusion fMRI [96], cerebral energy metabolism [97], and electrophysiological methods such as EEG [98] and MEG [99]. These findings suggest the presence of consistent and robust brain networks across various physiolog-

ical and imaging techniques.

Spatial Hierarchy in the Cortex

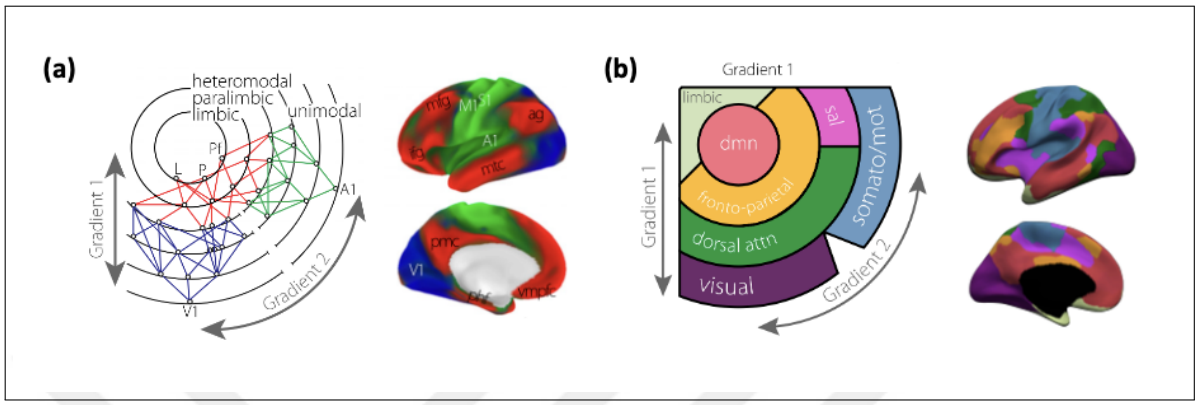

Figure 2.9 Cortical hierarchy defined by (a) Mesulam [6] and (b) Marguiles [15].

The human brain has a wide repertoire of complex functions enabled by its distinctive spatiotemporal organization (Figure 2.9). Marsel Mesulam was one of the first to suggest that brain processing is influenced by anatomical connectivity. Mesulam provided a detailed analysis of the neural pathways that link sensory information to cognition and proposed a hierarchy where distinct unimodal regions are coordinated by integrative transmodal areas [6]. Margulies and his colleagues have recently expanded this idea by offering a gradient-based view of hierarchical processing. They used a data-driven method to identify connectivity gradients in the brain [15]. By analyzing the main axes of variance in the connectivity matrix, they identified how different areas of the cortex are connected to one another, and how they are functionally ordered along specific gradients. They showed that the principal gradient of functional connectivity moves from sensory-motor areas to more complex association areas in the brain. In this hierarchy, they proposed a comprehensive organization of ICNs, placing the DMN at the top, sensory-motor networks at the lowest level, and attention networks in the intermediate zone. The exact mechanisms by which these three hierarchical layers interact to maintain a balance between integration and segregation are still not fully understood.

2.2 Frequency-Dependent Brain Dynamics

> As we take, in fact, a general view of the wonderful stream of our consciousness, what strikes us first is this different pace of its parts. Like a bird's life, it seems to be made of an alternation of flights and perchings.
>
> — William James

To adapt to dynamic environmental demands, the human brain coordinates complex processes across distinct spatial and temporal scales. The execution of higher cognitive functions relies on the accurate coordination of processes occurring at different time scales, both within and across functional brain networks. This idea of multi-time scale processing was initially conceptualized by William James in the late 19th century. In his insightful metaphor, James likened the stream of consciousness to a bird's life, alternating between flights and perchings [100]. Flights represent rapid, transient moments of thought, while perchings signify periods of reflection and integration. This metaphor has been further expanded by Deco et al. [101] within the framework of modern dynamical systems. Here, flights are associated with fast, segregative neural processes, and perchings with slower, integrative processes.

2.2.1 Time Scales of Brain Activity

> Clocks tick, bridges and skyscrapers vibrate, neuronal networks oscillate. Are neuronal oscillations an inevitable by-product, similar to bridge vibrations, or an essential part of the brain's design?
>
> — Buzsáki and Draguhn, 2004

Neural oscillations describe the rhythmic electrical activity that arises sponta-

neously or in response to stimuli from neuronal groups in the cortex [16, 102]. Communication within and between neural groups is achieved through oscillatory synchronization, which ensures coordinated rhythmic activity [102–105]. Electrophysiological techniques are extensively used to study neural oscillations, providing highly precise temporal resolution. Beyond accurate timing, these methods allow for distinguishing overlapping neuronal synchronizations across different time scales or frequencies, revealing key mechanisms of the neural integration [16, 102]. Neural oscillations have been shown to play an important role not only in cognitive processes [106, 107] but also in neurological and psychiatric disorders [108].

The mammalian brain generates a wide spectrum of neural oscillations, from very slow cycles lasting tens of seconds to rapid frequencies higher than 600 Hz. To organize this broad range of brain rhythms, Buzsáki and colleagues studied electrophysiological signals in rats (Figure 2.10, a) [16]. They grouped the different types of neural oscillations into ten oscillation classes, each representing a different frequency band. These frequency bands were found to have distinct characteristics and serve specific functions. However, there is still much to learn about their specific roles in cognition and how different oscillatory frequencies interact. A spatial pattern has also been observed in these types of oscillations: fast oscillations are typically restricted to smaller groups of neurons, whereas slow oscillations involve larger neural networks. Moreover, slower oscillations seem to modulate faster oscillations [109, 110].

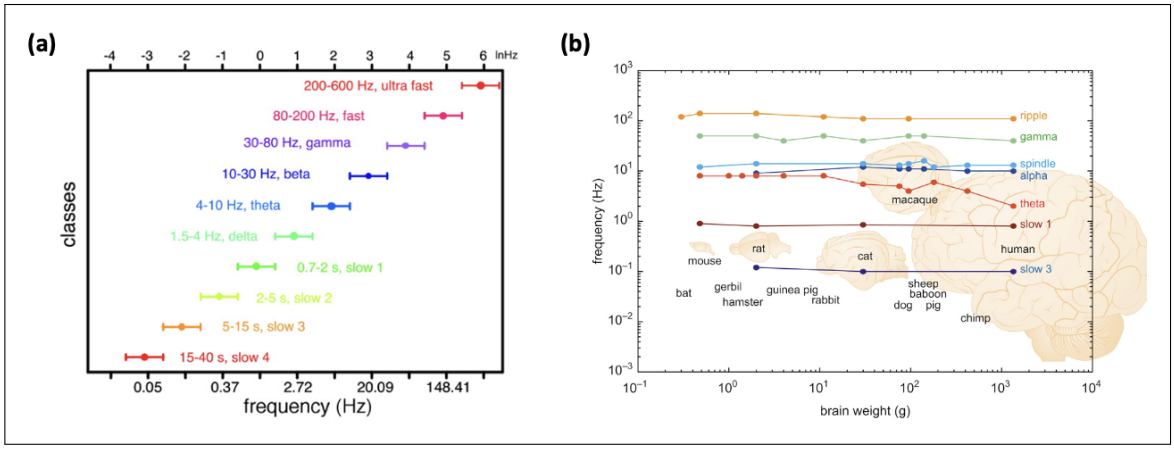

Figure 2.10 Time scales of brain activity. (a) [16]. (b) [17].

Evolutionary preservation of brain oscillations has also been observed across species (Figure 2.10,b). Buzsáki and colleagues found that oscillatory rhythms are present in nearly identical frequency ranges across various species, including humans, non-human primates, dogs, bats, gerbils, guinea pigs, rabbits, mice, and hamsters [17]. They also noted that this preservation of frequencies remains constant, regardless of brain size. Neural oscillations are typically divided into distinct frequency bands such as delta (0.5-3.5 Hz), theta (4-7 Hz), alpha (8-12 Hz), beta (13-30 Hz), and gamma (30-80 Hz), each of which is associated with different neural functions and behaviors.

Electrophysiology has improved our understanding of brain function by capturing high-frequency activity. However, methods like EEG have notable limitations, including poor spatial resolution and the inability to detect very slow frequencies ($<$ 0.5 Hz) [111]. In contrast, fMRI, despite its poor temporal resolution, is highly effective at mapping brain activity across the entire brain with high spatial resolution. Due to its low sampling frequency, fMRI is primarily suited to investigating a narrow range of frequencies, focusing on slow fluctuations.

2.2.2 Time Scales of Resting-State fMRI

fMRI's high spatial resolution and ability to capture slow brain activity make it an invaluable tool for investigating how large-scale brain networks support complex cognitive functions. However, since it serves as an indirect indicator of neural activity, the precise connection between these hemodynamic changes and actual neuronal activity is not fully understood [47].

It has been shown that the BOLD signal correlates strongly with single-neuron activity and the local field potential (LFP), which represents the combined electrical activity of neural populations at pre- and post-synaptic terminals [47, 112, 113]. Furthermore, a range of EEG- fMRI multimodal fusion studies showed that each one of those six ICNs identified by fMRI-based analyses was characterized by a specific combination of different brain rhythms such as delta, theta, beta, alpha, and gamma (Figure

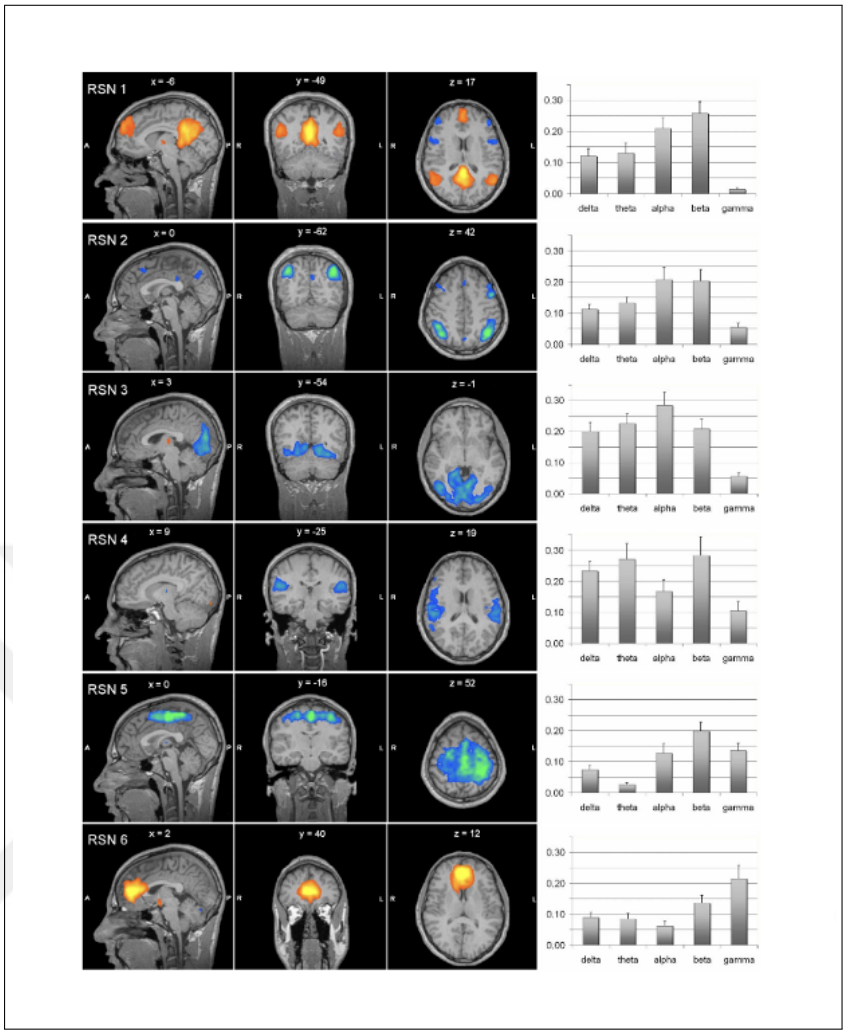

Figure 2.11 Oscillatory Signatures in ICNs [18].

2.11) [18, 114, 115]. These findings not only confirm that the BOLD signal represents meaningful neural activity, rather than noise, but also raise new questions about the potential multi-band frequency organization within the BOLD signal.

Most rs-fMRI studies focus on analyzing functional connectivity within a single broad frequency range (0.01 to 0.1 Hz) [7, 116, 117]. This approach introduces two limitations: it excludes higher frequencies from consideration and overlooks the potential frequency-specific features of the BOLD signal. Traditionally, frequencies above 0.1 Hz have been thought to originate primarily from non-neuronal sources, such as breathing and cardiac signals [118, 119]. However, recent research indicates that higher frequencies (>0.1 Hz) carry significant neuronal information [120]. Moreover, there is also evidence of frequency-specific patterns in FC [19, 43] as well as in other features of the

BOLD signal such as regional homogeneity (ReHo) [44], amplitude of low- frequency fluctuations (ALFF) [121] and power [122, 123].

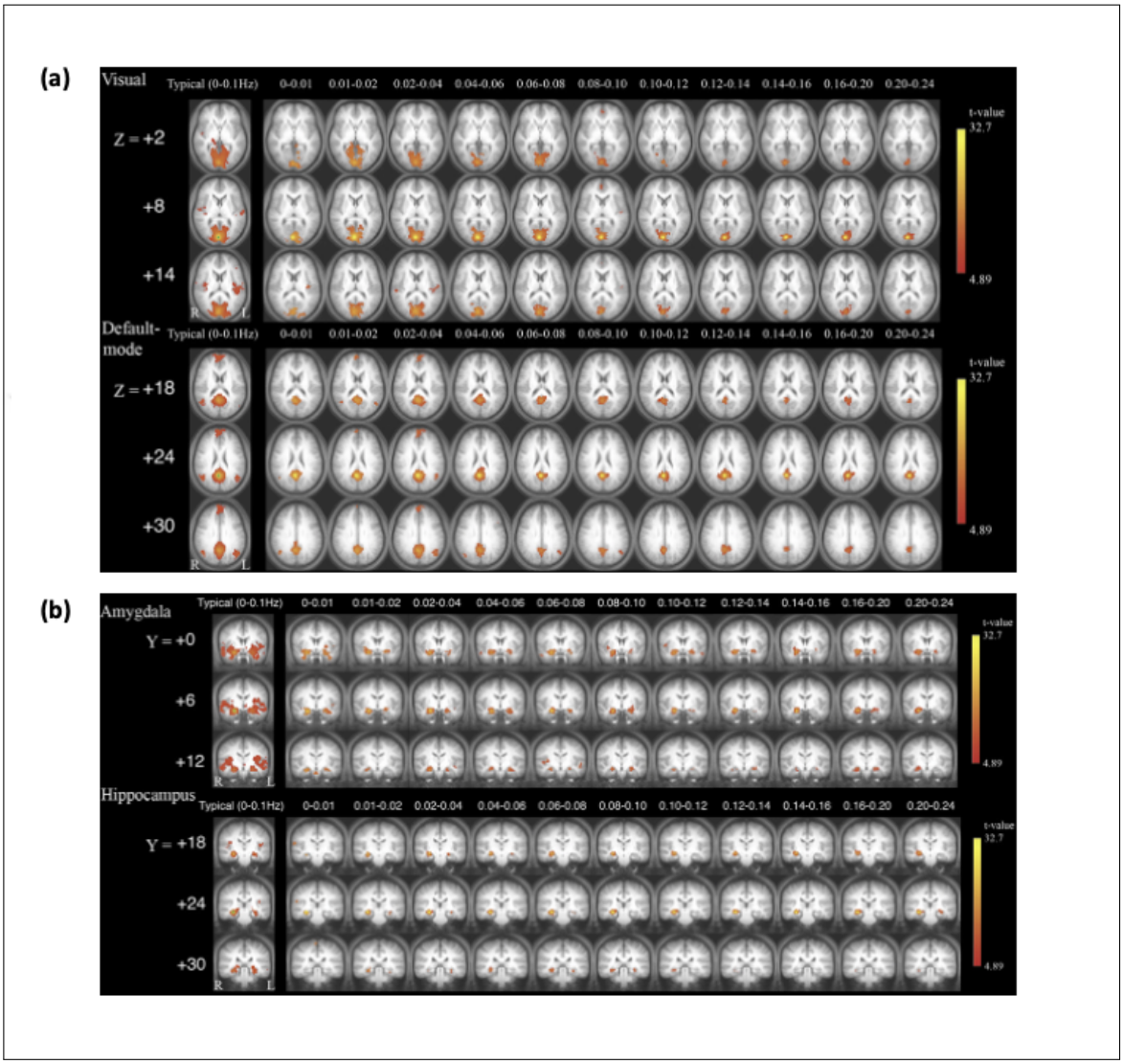

Figure 2.12 Frequency-specific connectivity maps of (a) visual system and default-mode network (b) amygdala and hippocampus [19].

Wu and colleagues are one of the first groups to examine the existence of frequency-specific characteristics in the resting-state fMRI signal (Figure 2.12,a) [124]. They investigated five brain networks by decomposing them into 12 frequency bands within the frequency range of 0-0.24 Hz. Results showed that cortical networks tend to operate within the ultra-low frequency range (0.01-0.06 Hz), while connections in limbic networks span a broader range (0.01-0.14 Hz). Another group studied the spatial distribution of fluctuations across different frequency ranges for various regions of

interest [123]. They showed that cortical regions exhibit the highest contribution of low-frequency signals (<0.25 Hz), while time courses in subcortical regions and the insula, are strongly influenced by higher-frequency fluctuations (0.25-1.4 Hz). While these studies used exploratory frequency ranges without any assumption, some attempted to identify important frequency ranges by considering the spectral or topological properties of the resting brain [125–127].

The most commonly used frequency bands are slow-5 (0.01-0.027 Hz), slow-4 (0.027-0.073 Hz), slow-3 (0.073-0.198 Hz), and slow-2 [127]. Inspired by the oscillation classes defined by Buzsáki and Draguhn [16, 102], Zuo and colleagues were the first to decompose the resting-state BOLD signal into these four frequency bands [121]. However, since these frequency bands were originally defined based on electrophysiological recordings in rats, they may not provide the most accurate classification for analyzing resting-state fMRI signals in humans [126].

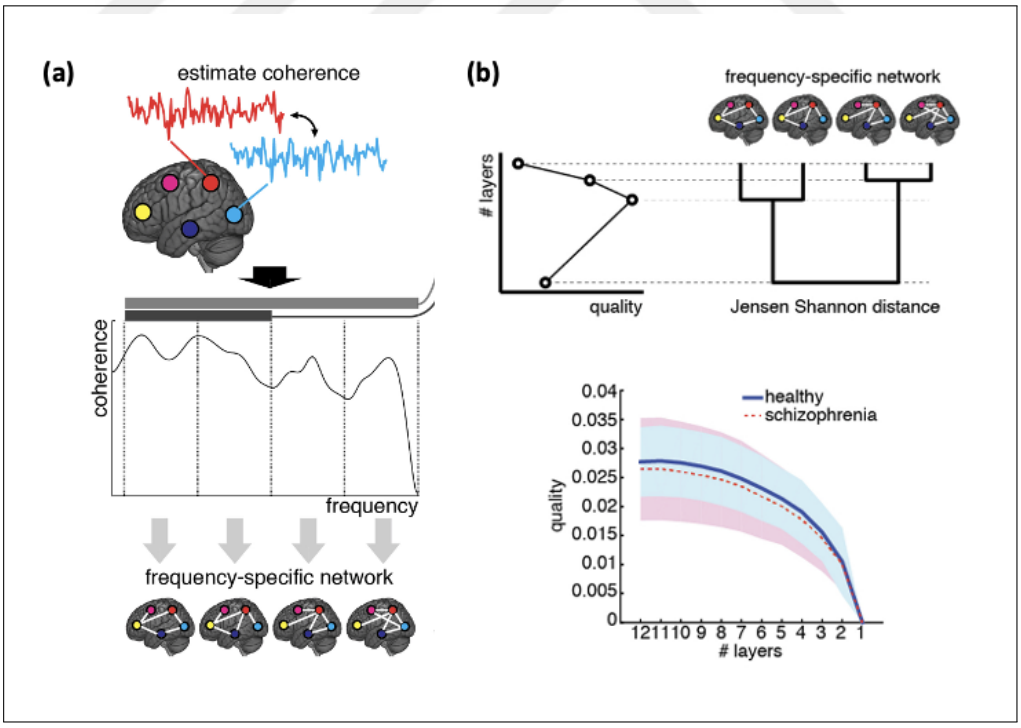

Figure 2.13 (a) Multilayer framework and (b) structural reducibility method used by De Domenico et al. [20].

De Domenico et al. (2016) suggested analyzing brain activity and network topology using a multilayer network approach which allows the study of frequency-

specific information across different layers simultaneously [20]. In this approach, the connectivity network for each frequency band corresponds to a layer. Each node (brain region) is connected to its counterparts in all other layers, corresponding to different frequency bands. Before proceeding with further analysis, they first examined whether all frequency layers were necessary to capture the key organizational properties of brain networks. To do this, they applied their structural reducibility method, which assesses how much unique topological information each layer of a multiplex network contributes, compared to the aggregated network model [128]. De Domenico et al. demonstrated that brain networks derived from fMRI across different frequency bands are difficult to reduce, as each layer provides unique topological information (Figure 2.13). This means that even though high-frequency fMRI oscillations may be underrepresented, their interaction across all layers is essential for brain functioning. They also showed that hubs in the multilayer network are distinct from the ones in conventional analysis. A more accurate identification of key brain regions could enhance the ability to differentiate between healthy individuals and those with schizophrenia.

2.2.3 Temporal Hierarchy in the Cortex

Human cortical regions follow a sensorimotor-to-transmodal gradient, where brain areas progress from simpler sensorimotor functions to more complex transmodal areas involved in higher-order cognition. This gradient reflects a gradual variation in structural properties, such as cytoarchitecture, myeloarchitecture, and connectivity, as well as functional specialization [15, 129, 130]. It is reasonable to anticipate that these anatomical gradients will be reflected in corresponding patterns of brain activity and function. Murray and colleagues [131]. suggested a hierarchical organization in the brain's cortical areas based on the timescales of intrinsic fluctuations. They analyzed the autocorrelation of spiking activity in primate brains to measure these time scales. Results showed that sensory areas, responsible for processing immediate stimuli, exhibit fast fluctuations. In contrast, higher-order areas like the prefrontal cortex, involved in more complex processing, have slower fluctuations. The hierarchical organization of brain time scales, originally observed in non-human primates, has been validated in

human data using fMRI [132, 133]. They confirm that unimodal areas, such as sensory and motor regions, exhibit faster neural dynamics, while transmodal regions, including the CEN, DAN, and DMN, responsible for higher-order functions, display slower neural activity.

2.3 Complex brain networks

> The genesis of mathematical creation is a problem, which should intensely interest the psychologist. It is the activity in which the human mind seems to take least from the outside world, in which it acts or seems to act only of itself and on itself, so that in studying the procedure of geometric thought we may hope to reach what is most essential in man's mind.
>
> — Henri Poincaré, 2009

Poincaré suggests that mathematical creation arises from internal processes of the mind, independent of external stimuli, which resonates with the way the brain organizes itself. On the other hand, in network neuroscience, brain organization is often studied via graph theory, where the brain is modeled as a network of interconnected regions (nodes) and their connections (edges).

While Poincaré suggests that the way the mind organizes and manipulates abstract ideas, such as geometric shapes and mathematical theorems, can reveal fundamental aspects of how human cognition works, network neuroscience applies similar mathematical abstraction to explore the brain's structural and functional organization. In a way, this closes the loop: just as examining the mechanism behind abstract thought helps us understand the mind, mathematical tools like graph theory allow us to uncover how the brain itself is organized to support such abstract thought. This

interplay between abstract mathematics and brain function forms a fascinating bridge between the mind's creative processes and its underlying biological mechanisms.

2.3.1 Connectivity as a Graph

> This question is so banal, but seemed to me worthy of attention in that neither geometry, nor algebra, nor even the art of counting was sufficient to solve it.
>
> — Leonhard Euler, letter of March 1736

The foundations of network neuroscience can be traced back to Euler's ingenious work on the Königsberg bridge problem, which asked whether it was possible to cross all seven bridges without retracing any steps [34]. Euler admitted that the problem of crossing seven bridges in Königsberg seems like a simple, almost trivial puzzle [22]. Despite this simplicity, he found it intriguing because it could not be solved using traditional mathematical methods like geometry, algebra, or counting.

Euler considered this problem to be related to what Leibniz called "geometria situs," or the geometry of position [134]. His breakthrough insight was realizing that the problem could be reduced to the connections between regions (nodes) and bridges (edges). By abstracting the physical landscape, Euler transformed the problem into a graph, where only the relationships between nodes and edges matter, not the physical layout. He observed that for a path to cross all bridges without repeating any, only two nodes can have an odd number of links, which would serve as the start and end points. If a node with an odd number of links is encountered, it leaves no unused link to exit. Since the Königsberg graph had four nodes with odd links (A, B, C, and D), such a path was impossible (Figure 2.14).

His solution to this seemingly simple puzzle laid the foundation for graph theory, a pivotal mathematical framework that later expanded into the field of topology.

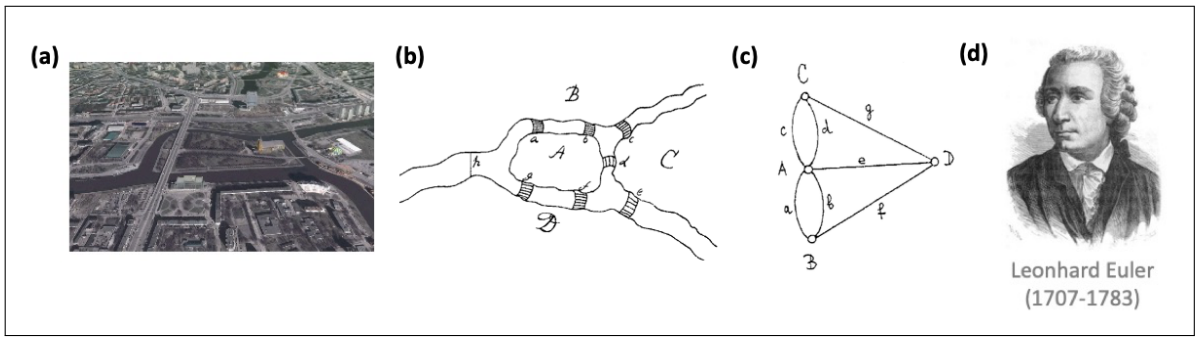

Figure 2.14 From Königsberg's seven bridges (a) to Euler's graph (c). The graph is composed of four nodes (A, B, C, D), representing the path of lands, and seven edges, each representing a bridge connecting these regions. (a) From the book Network Science written by Barabasi [21]. (b) From Euler's letter to Carl Leonhard Gottlieb Ehler (1736). (c) From from Euler's paper [22].

On one hand, graph theory is a pure mathematical subject. It explores abstract concepts like graph coloring, connectivity, and algorithms, which may not have immediate practical applications. On the other hand, applied graph theory has numerous real-world uses in areas such as computer science, social network analysis, and network neuroscience [135–137].

A graph $G = (V, E)$ is defined by a set of vertices V and edges $E \subseteq V \times V$. The number of vertices $|V|$ is called the graph's *order*, and the number of edges $|E|$ is its *size*. If two vertices $v_1, v_2 \in V$ are connected by an edge, they are called *adjacent*. Similarly, edges that share a vertex are adjacent. A *loop* is an edge that connects a vertex to itself. The *degree* of a vertex is the number of edges incident to it, with loops counted twice, and is denoted $\deg(v)$. A *simple graph* has no loops or parallel edges, and most network neuroscience studies focus on simple graphs.

Networks are typically represented by *adjacency matrices*, where nodes are in the rows and columns, and the edges are the matrix entries. An entry $a_{ij} = 1$ indicates an edge between vertices v_i and v_j; otherwise, $a_{ij} = 0$. These matrices are used in subsequent graph-theoretical analysis. In a simple graph with no loops, the diagonal entries must be zero, and for undirected graphs, the adjacency matrix is symmetric. Additionally, graphs can also represent *weighted networks*, where edges represent the strength of the connections. Weighted networks allow for a more nuanced analysis of

connections and are commonly used in network neuroscience.

2.3.1.1 Defining Nodes and Edges

In brain networks, nodes generally represent brain regions or sensors, such as regions of interest (ROIs) in fMRI, electrodes in EEG, and sensors in MEG. Parcellation schemes are often used to define these nodes. Various parcellation methods have been developed by different research groups, incorporating anatomical features, clustering techniques, and machine-learning approaches (Figure 2.15) [138].

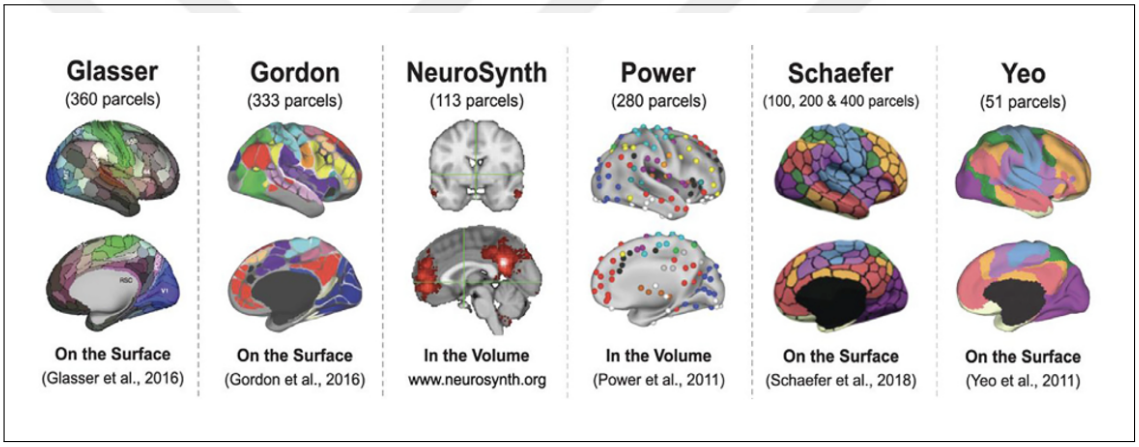

Figure 2.15 Parcellation schemas [23].

Defining nodes is relatively straightforward, but the characterization of edges is more complex. Different types of connectivity can be represented by edges, including structural, functional, or effective connectivity. Structural connectivity describes the white matter tracts linking brain regions, often detected through diffusion tensor imaging (DTI). Functional connectivity captures the temporal dependencies between spatially distant brain regions, usually estimated using fMRI data. Effective connectivity indicates causal relationships, either direct or indirect, between brain regions and is widely used in EEG/MEG analyses. Functional connectivity in fMRI can reflect both linear and nonlinear interactions at various time scales. Correlation-based techniques, especially Pearson's correlation coefficient, are the most common [139]. These techniques measure the linear relationship between time-series data from different brain regions, helping to reveal how different parts of the brain work together during specific

tasks and behaviors. However, there are notable limitations with correlation-based methods, especially when dealing with more complex, nonlinear brain interactions.

In their exploratory study, Mohanty and her colleagues investigated whether traditional methods of measuring functional connectivity (FC) were sufficient and whether alternative measures could provide a more comprehensive view (2020). They examined eight alternative FC measures. Their preliminary findings suggest that:

- Pearson's correlation may not fully capture its complexity.
- Several alternative methods can assess brain signal interactions in different ways.
- No single FC measure is clearly superior for classification or prediction tasks.
- Large-scale brain connectivity, often defined by Pearson's correlation, may appear differently when using other FC definitions.

Phase-based connectivity measures, unlike standard correlations, are particularly adept at uncovering interactions that occur within specific frequency bands. This has significant implications, as brain function is often organized within distinct frequency ranges, each potentially carrying different types of cognitive information [16]. Studies have shown that phase-based connectivity measures can reveal finer functional subregions and exhibit better classification performance in machine learning tasks, suggesting that these frequency-domain methods provide richer insights than their time-domain counterparts [140].

In summary, while correlation-based methods are useful for linear interactions, phase-related can better capture the intricate dynamics of brain connectivity, especially when studying complex, frequency-specific neural processes.

Edges can also vary by weight (binary or weighted) and directionality (directed or undirected). In structural networks, weights mostly indicate the density of tracts, while in functional or effective networks, they represent the strength of interactions [24].

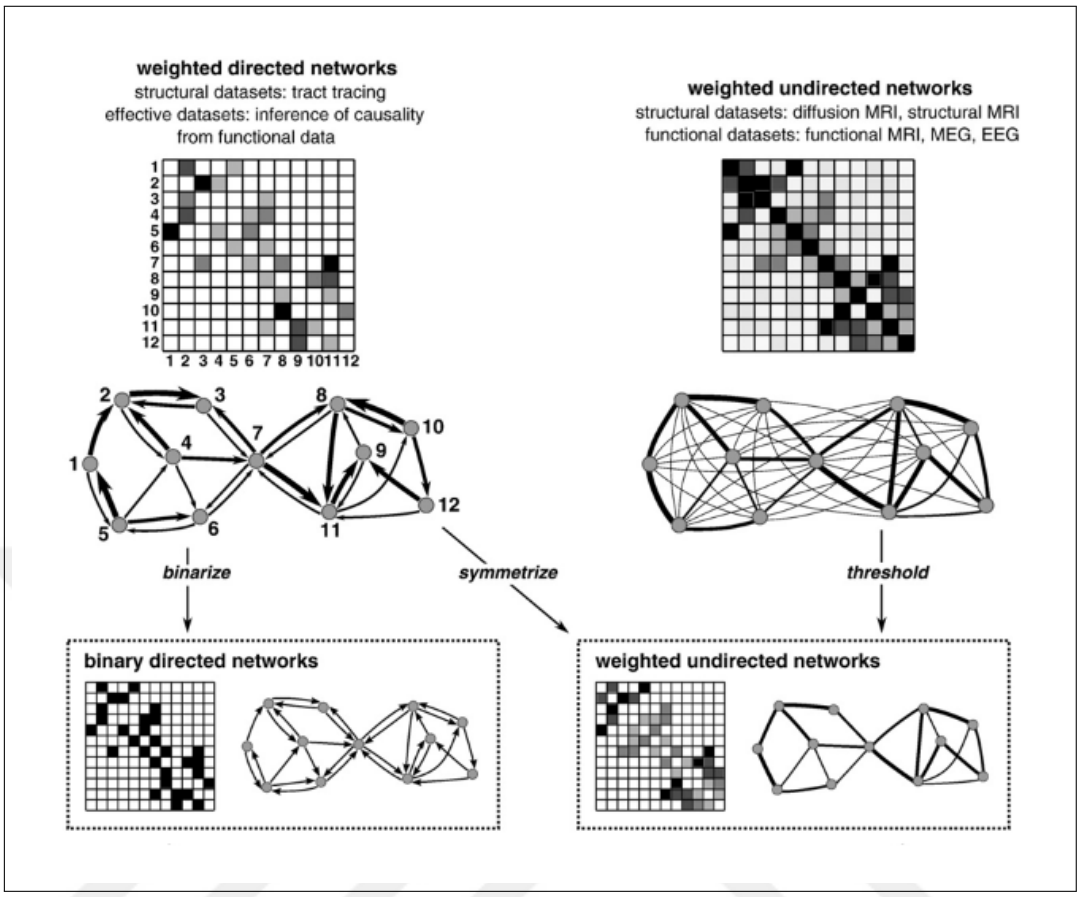

Figure 2.16 General pipeline for building graph from connectivity [24].

Binary edges only show the presence or absence of a connection, often identified through thresholding techniques (Figure 2.16).

2.3.1.2 Measures of Brain Networks

Graph theoretical analysis provides various quantitative metrics to assess the organization of networks (Figure 2.17) [24]. Global metrics, such as characteristic path length and small-worldness, give information about the whole network. Nodal metrics, such as degree, strength, betweenness centrality, and participation coefficient, provide insight into the importance of individual nodes in network connectivity and the flow of information. Modularity, positioned between these two scales, indicates how efficiently a network is divided into distinct, densely interconnected groups of nodes, providing insight into local specialization and global integration.

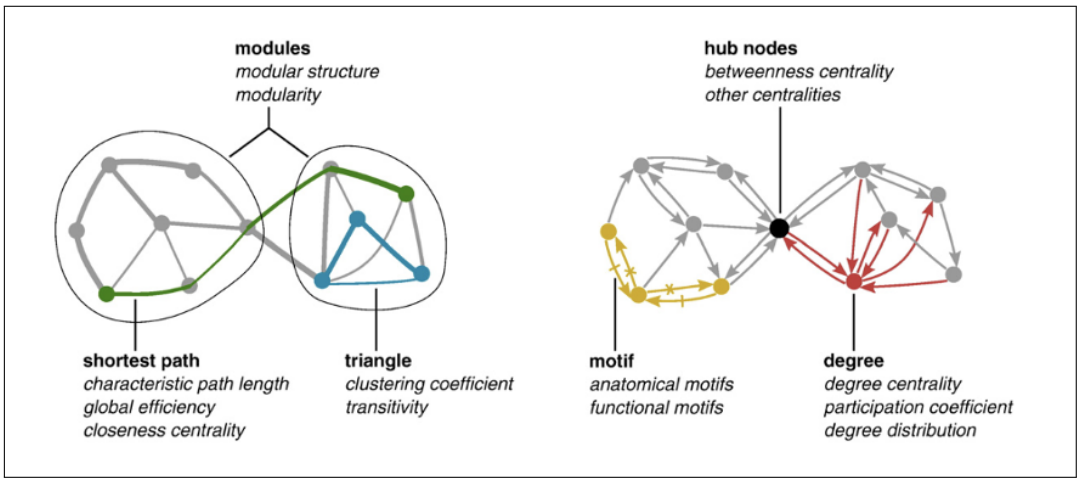

Figure 2.17 Fundamental graph metrics [24].

Fundamental network properties include:

- **Clustering Coefficient:** Measures local clustering; a higher value indicates a more segregated network.
- **Characteristic Path Length:** Represents the efficiency of information transfer.
- **Small-Worldness:** Balances clustering and path length, compared to random networks.
- **Global and Local Efficiency:** Assess information flow efficiency globally or locally within subnetworks.
- **Modularity:** Describes how well the network is divided into distinct communities.

2.3.2 Graph metrics on integration and segregation

Functional segregation involves the processing of information within groups of brain regions that are functionally related. In brain networks, these groups of regions are referred to as "modules" or "communities," where nodes within a community are tightly interconnected, while connections between different communities are limited (Figure 2.18, a). These modular structures are key features of complex systems [141]

and are believed to be essential for understanding cognitive processes and mental function [142]. In the brain, these interconnected communities exist across multiple levels, from individual brain regions to functional circuits to large-scale networks. Communities can be objectively identified using a wide range of algorithms [143].

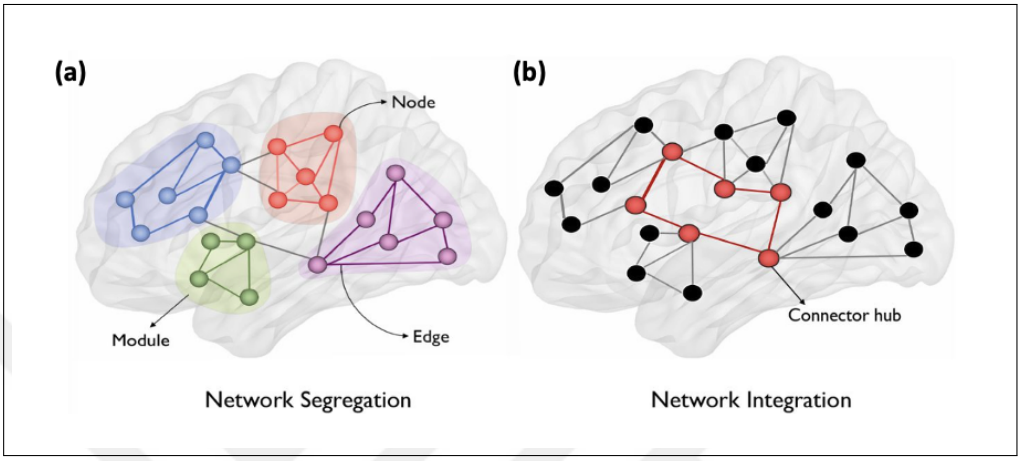

Figure 2.18 Figurative explanation graph metrics related to segregation and integration [25].

Functional integration in networks can be considered in two main ways: by assessing global communication efficiency [144] and the network's ability to combine information from distributed regions. Global efficiency is the average shortest path length between any two nodes in the network. This measure tends to be highest in networks with a random structure, which lacks clear community organization, leading to less segregation of information. On the other hand, central brain regions representing "network hubs" promote the integration of information but can also exist in highly segregated networks (Figure 2.18, b).

2.3.2.1 Modularity

Newman and Girvan [145] outlined two main criteria for assessing the quality of partitions in network analysis: (1) nodes within the same module should be highly interconnected, and (2) the internal connectivity of a module should surpass what would occur by chance. The configuration model, often used in modularity analysis, preserves the degree sequence of the network and helps estimate network properties across randomized graphs [146]. Modularity algorithms produce a partition M, which

defines the module assignments of the parcels, and an index Q, which quantifies the quality of the modularity.

$$[Q, M] = \frac{1}{2} W \sum_{i,j} (w_{ij} - \gamma e_{ij}^{w}) \delta(m_i, m_j) \tag{2.1}$$

where w_{ij} is the weight of the edge linking node i and j, and $W = \frac{1}{2} \sum_{i,j} w_{ij}$ is the total weight of edges of the network. The weight of edges connecting nodes in the same community expected by chance is given by $e_{ij}^{w} = \frac{s_i s_j}{2W}$, where s_i and s_j are the sums of the weights to nodes i and j, respectively. The function $\delta(m_i, m_j)$ is set to 1 when nodes are in the same community and 0 otherwise.

The Louvain algorithm is a well-known method developed by Blondel (Figure 2.19) [147] to find partitions that maximize modularity in networks. The process follows five essential steps:

1. Start by considering each node as a distinct module.
2. Randomly choose a node, calculate the change in modularity Q from merging it with an existing module, and perform the merge that produces the largest increase in Q.
3. Repeat step 2 until no additional increase in Q occurs, revisiting nodes as necessary.
4. Merge nodes within the same module into "super nodes," creating a meta-network. Here, edges between super nodes represent inter-module connections, and the connectivity within a super node is indicated by a self-loop.
5. Continue repeating steps from 2 to 4 until no additional improvements in Q occur.

Advantages of the Louvain Algorithm

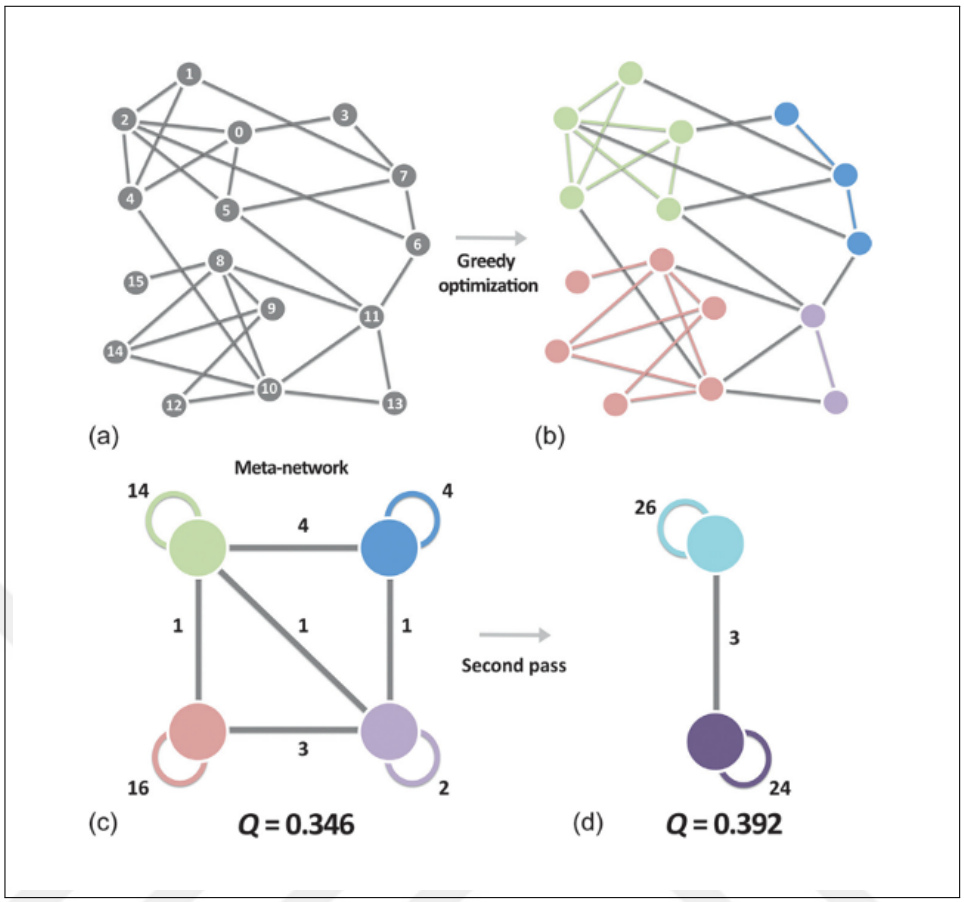

Figure 2.19 The Louvain algorithm for community detection [26].

The algorithm is highly efficient, making it applicable to large networks. It is more accurate than many other community detection methods. Moreover, it can be used to explore hierarchical structures, effectively addressing the resolution limit problem of other modularity optimization methods.

Limitations of Modularity

Degeneracy of Modularity Maximization: The Louvain algorithm, which is stochastic, can yield different results with each run. Consensus clustering addresses this by combining the outputs of these different partitions into one representative partition.
Resolution Limit: Standard algorithms may miss smaller communities. To address this, a tunable resolution parameter is used, allowing the algorithm to detect smaller or larger communities. However, selecting an appropriate resolution parameter can be arbitrary.

Nonzero Q Values in Non-Modular Networks: Even non-modular networks can produce high Q scores due to sampling variations, which require validation to ensure statistical significance. Benchmarking against randomized networks helps confirm the statistical significance of Q values by comparing empirical network scores to those generated in randomized trials.

Consensus Clustering

One limitation of modularity metrics is the existence of numerous distinct partitions that are nearly equally optimal, referred to as degenerate solutions [27]. Given the noisy nature of empirical network topology estimates, selecting a single "optimal" partition as the representative structure can seem arbitrary. Instead, these degenerate solutions should be combined into consensus partitions. This can be achieved by creating an agreement matrix that is repeatedly reclustered until a single consensus partition is formed (Figure 2.20) [28].

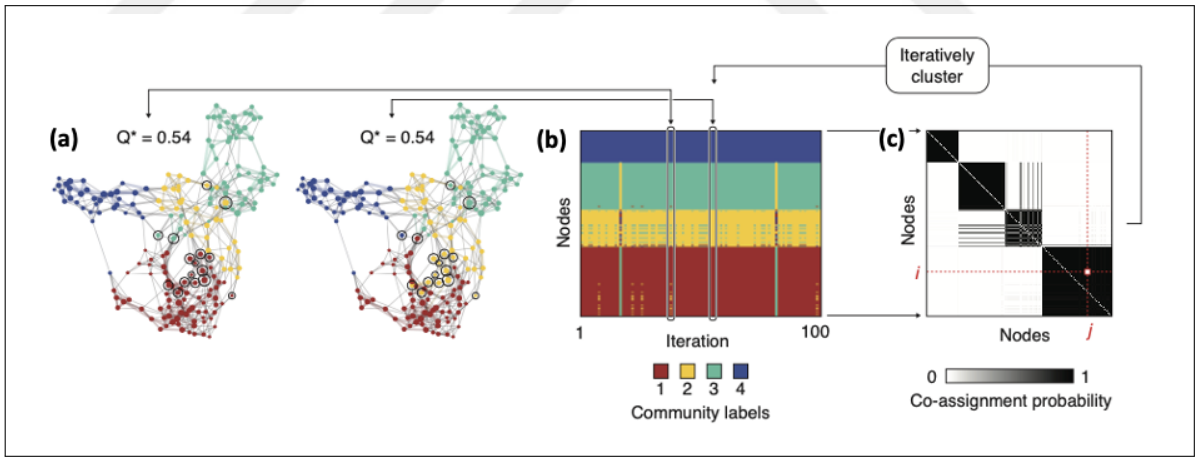

Figure 2.20 Consensus clustering algorithm [27, 28]. Two partitions with approximately the same quality ($Q = 0.54$) might show different community assignments.

When the Louvain algorithm is run 100 times, multiple solutions can appear. To solve this problem, consensus clustering generates an agreement (co-assignment) matrix from these multiple runs. Each element of the matrix records how frequently a pair of nodes is placed in the same community across different partitions. This matrix is then reclustered using modularity maximization, estimating the co-assignment of

two nodes based on a null model (where node assignments are random). Therefore, consensus clustering involves two iterative steps: constructing the co-assignment matrix and clustering it. After a few iterations, the process converges to a representative partition.

2.3.2.2 Participation Coefficient

The participation coefficient is a network metric that quantifies how a node's connections are distributed across different modules. Nodes with high participation coefficients have connections spread across multiple modules, while nodes with low participation coefficients are primarily connected within their own module.

According to Guimerà and Amaral [148], the participation coefficient P_i of a node i is calculated as:

$$P_i = 1 - \sum_{m=1}^{M} \left(\frac{k_i(m)}{k_i} \right)^2 \tag{2.2}$$

where M is the number of modules in the network, $k_i(m)$ is the number of links between node i and other nodes in module m, and k_i is the degree between node i and all other nodes in the entire network.

A participation coefficient of 0 means that all of a node's connections are within one module, indicating a specialized role. A value near 1 implies the node has connections spread across multiple modules, suggesting the node functions as a bridge between different communities. This metric is crucial for identifying important nodes that help facilitate communication and integration across the network. Nodes with high participation coefficient values are called connector hubs.

Previous research has demonstrated that brain networks contain connector hubs

[149, 150] that are highly active during task execution [151] and serve as key links between different networks [31, 152, 153]. These findings suggest that connector hubs play a crucial role in facilitating the interaction between control and processing networks, which is essential for complex cognitive functions [152].

2.3.2.3 Flexibility

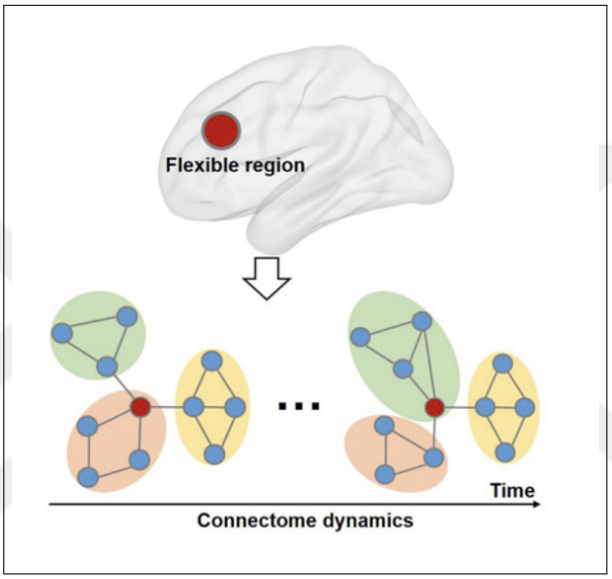

Figure 2.21 Flexibility [29].

Flexibility in brain networks refers to the ability of a brain region or "node" to change its modular affiliation over time. In other words, it is the extent to which a node shifts between different functional communities or networks during dynamic brain activity (Figure 2.21) [154].

$$\text{flex}_i = \frac{n}{N-1} \tag{2.3}$$

where n represents the number of distinct modular assignments for node i across various frequency bands, while N denotes the total number of time points.

In Bassett et al. [154], flexibility was used to study the time-varying dynamics of functional connectivity during a motor learning task. They measured how brain

regions switched their community affiliations across different time windows during the task, focusing on the "temporal core" and "temporal periphery" of the brain network. Their findings emphasized that brain regions with high flexibility were primarily located in association areas, which were crucial for higher cognitive functions such as learning and memory formation. This underscores the importance of flexibility in facilitating complex cognitive tasks.

3. MATERIALS AND METHODS

3.1 Data

This study was carried out using data from the Human Connectome Project (HCP) database [155]. Data collection and sharing have been authorized by the HCP parent Institutional Review Board (IRB). Data Use Terms were signed and approved by the WU-Minn HCP Consortium. We used two sequences: structural MRI (T1-weighted, 256 slices, 0.7 mm^3 isotropic resolution, TE = 2.14 ms, TR = 2400 ms, TI = 1000 ms, flip angle = 8°) and resting-state fMRI (gradient-echo EPI, TR = 720 ms, TE = 33.1 ms, flip angle = 52°, FOV = 208 × 180, voxel size = 2 mm isotropic). Each rs-fMRI run, lasting 14 minutes and 33 seconds, contains 1200 frames. During the resting-state scan, participants were instructed to fixate their eyes on a projected bright cross-hair on a dark background. The MRI and behavioral data were collected on two consecutive days. Here, we only used the data from the first scanning session, in the LR direction.

3.2 Preprocessing

We used the minimally preprocessed ICA-FIX processed data on fs LR32K surface space from 98 subjects [155]. Some recent studies reported that the ICA-FIX algorithm was insufficient to eliminate motion artifacts and recommended further preprocessing methods such as global signal regression (GSR) and CompCor methods [156–159]. For such further preprocessing, we used minimally preprocessed volume data of the same subjects which we processed by using the CONN toolbox [160]. Initially, we calculated framewise displacement (FD) using the derivatives of the six rigid-body transformation parameters obtained from the realignment step [161] and the root-mean-squared change in the BOLD signal from volume to volume (DVARS). Rules as FD > 0.5 mm or DVARS > 5% were used to identify the outlier frames, and participants

having DVARS greater than 20% of 1200 frames were excluded from further analysis (2 subjects).

After this step, in order to estimate the nuisance covariates, we applied the CompCor approach that is described by Behzadi et al. [162] and implemented in the CONN toolbox. According to this approach, the first five principal components from each of the white matter (WM) and the cerebrospinal fluid (CSF) signals are used to estimate the noise contribution to the fMRI signal. We preferred the CompCor strategy over the GSR for removing noise from the fMRI data since GSR by including the global gray matter (GM) signal can introduce spurious negative correlations and alter the true connectivity structure in the fMRI data [163]. CompCor targeting more specifically the noise components without removing potentially useful global GM signals offers a robust alternative to GSR [164]. For more reliable estimation of the noise components expressed in the WM and CSF signals, an initial step of eroding the WM and CSF segments has been applied to avoid any contribution from GM borders (binarization threshold = 0.5, erosion steps = 4, and erosion neighborhood = 9).

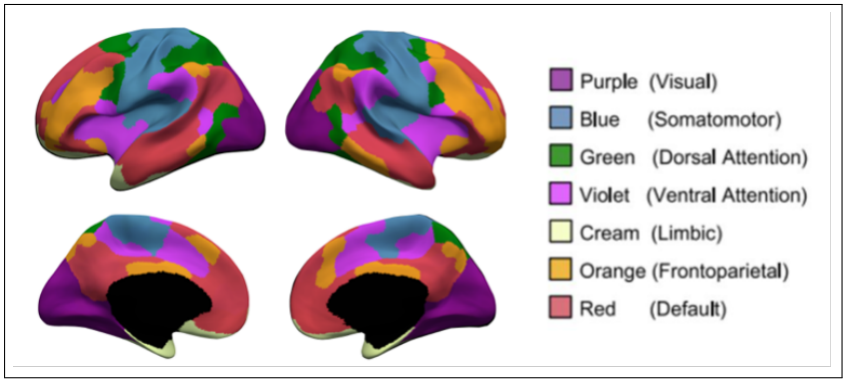

Figure 3.1 Schaefer's parcellation (400 parsel, 7 network) [30].

Finally, a total of 24 independent variables, including the six movement parameters, their derivatives, the 5+5 principal components from CompCor, FD, and DVARS were used to regress out noise from the surface data by a general linear modeling (GLM) step. To obtain the time series for regions of interest (ROIs), the residual waveforms belonging to each parcel were averaged using Schaefer's atlas (Figure 3.1) [30]. Therefore, we obtained 400 parcel waveforms on the cortex, each of which was assigned to one of the seven ICNs. Each parcel time series was detrended before any further anal-

ysis. After the preprocessing, a time series matrix with dimensions 400×1200 for each participant was obtained (Figure 3.2).

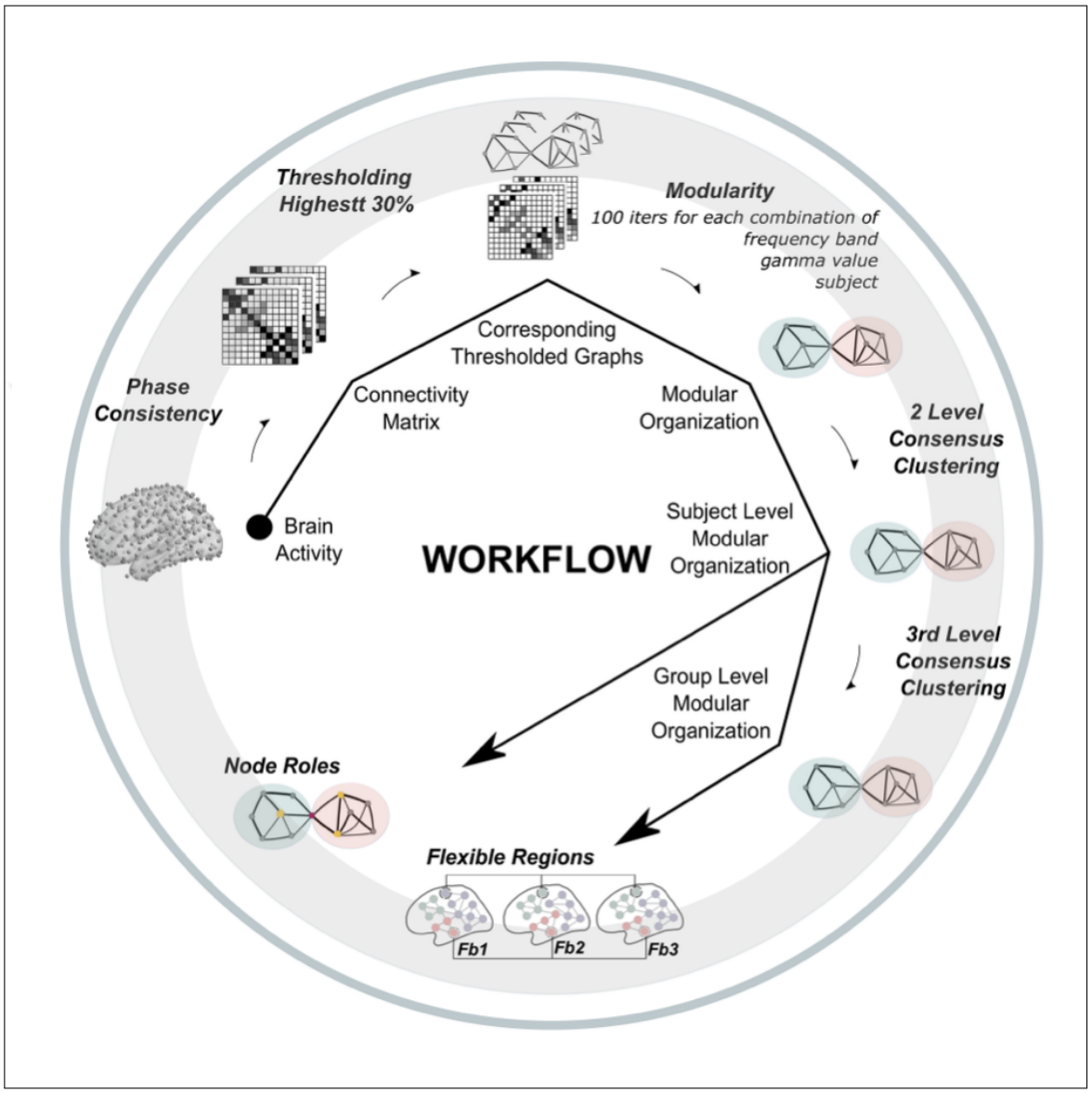

Figure 3.2 Workflow overview. First, we calculated phase consistency matrices and thresholded them. Then, we performed a modularity analysis followed by twofold consensus clustering to determine the subject-level modular organization and a third-fold one to identify the group-level modules. We utilized the results of the group-level modular organization to define the flexible regions over frequency bands. We examined the connector role of brain regions in the network by calculating the normalized participation coefficient for each parcel using subject-level information. Finally, we studied the relation of these node-specific graph metric values of integrative and core regions to high-order cognition.

3.3 Connectivity Estimation

We studied phase locking to assess the consistency of phase differences between parcel pairs over time windows in specific frequency bins. We referred to this index as "Phase Consistency" (PC, eq. (2)) as a more general term for phase synchronization [165].

Fourier transform was applied to the signals, and phase information was obtained for each frequency component as

$$\text{Fourier}(x(n)) = \sum_{n=0}^{N-1} x(n)e^{-j2\pi fn} = A(f)e^{\phi(f)}. \tag{3.1}$$

where $x(n)$ denotes the time series of a parcel and $A(f)$ and $\phi(f)$ represent its amplitude and phase at a specific frequency bin f, respectively. To reduce estimation variance, we used 15 sliding windows with 50% overlap. Fourier transform was applied to each time window consisting of 150 data points, which encompassed one full oscillation cycle of the lowest frequency component in the range examined (0.01-0.1 Hz). The TR of the BOLD signal was 0.72 sec, and the data was zero-padded to 256 points to use FFT for efficient computation, yielding a frequency resolution of $\Delta f = \frac{1}{0.72\times256} = 0.0054$, corresponding to the width of each frequency bin. The resulting frequency domain representation of each epoch yielded 18 frequency bins covering the 0.01-0.1 Hz interval. Phase differences between all parcel pairs calculated at 18 frequency bins in the range 0.01-0.1 Hz for 15 windows were stored as a four-dimensional tensor ($parcel \times parcel \times frequency \times window : 400 \times 400 \times 180 \times 15$) for each participant.

A serious drawback related to the phase-related connectivity metric is that there might be a bias toward positive values if the sample size is small [165], which decreases rapidly with the number of samples and becomes negligible for $N > 50$ [166]. Therefore, we reduced the frequency range into three bands and increased the sample size by a factor of six to obtain unbiased PC estimates in the frequency range of interest.

Phase difference values were converted into unit vectors in the complex plane and were averaged over 15 windows and six frequency bins, resulting in a vector for each frequency band (0.011-0.038 Hz, 0.043-0.071 Hz, or 0.076-0.103 Hz).

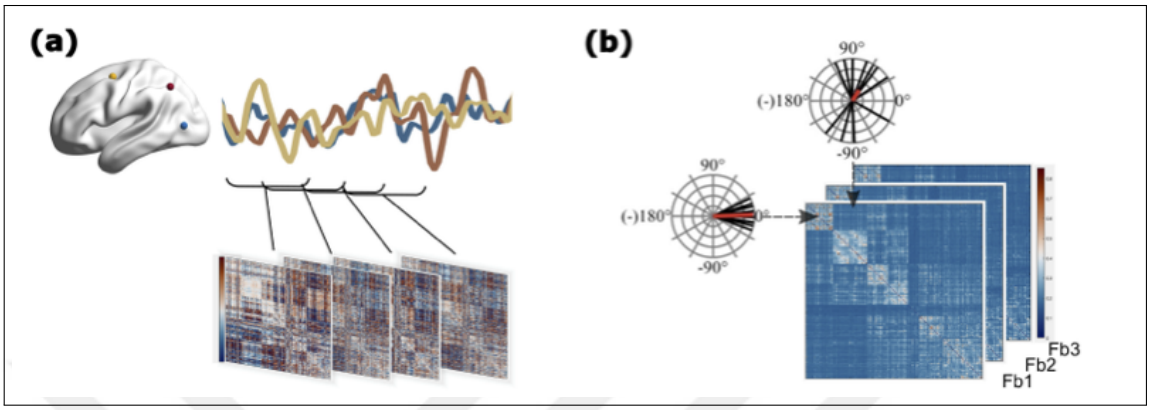

Figure 3.3 Phase differences between parcel pairs were calculated for each time window and frequency bin (a), these phase difference matrices were used to compute phase consistency for three frequency bands (b). PC, Phase Consistency; Fb1, 0.011-0.038Hz; Fb2, 0.043 - 0.071Hz; Fb3, 0.076 - 0.103Hz.

The magnitude of this resultant complex vector was defined as parcel-based phase consistency and its angle as phase difference (PD). The analysis yielded a pair of tensors (parcel × parcel × frequency band: 400 × 400 × 3, Figure 3.3) for each subject. We computed PC_{ij} and PD_{ij} for each frequency band as follows:

$$\mathrm{PC}_{ij} = \left| \frac{1}{FK} \sum_{f=1}^{F} \sum_{k=1}^{K} e^{i(\phi_i(f,k) - \phi_j(f,k))} \right| \tag{3.2}$$

$$\mathrm{PD}_{ij} = \tan^{-1} \left(\frac{1}{FK} \sum_{f=1}^{F} \sum_{k=1}^{K} e^{i(\phi_i(f,k) - \phi_j(f,k))} \right) \tag{3.3}$$

where i and j were parcel pair indices, f was the frequency bin index, and k was the time window index with $F = 6$ and $K = 15$.

We identified an optimum threshold so that the networks had the small-worldness property with the largest connected component remaining intact, in turn preserving the network's structure while discarding the potential effects of noise. By using syn-

thetic as well as real-world networks, Bordier and coworkers ([167] have shown that percolation analysis can be used to identify the optimal sparsification threshold, which maximizes the information extracted by the community detection algorithm.

3.3.1 Identifying the Optimum Sparsity Level

We identified the optimum threshold for the networks to have the small-worldness property and the largest connected component to stay intact so the network's structure was preserved while discarding the potential effects of noise. We have started with a set of proportional thresholds between 5% and 40% defined on the grounds of the existing literature reported small-worldness of neuroimaging-based brain networks [168, 169]. First, we calculated the small-worldness index for each sparsity level (40%, 30%, 20%, 10%, and 5%) to guarantee the small-worldness property (Figure 3.5, a). Then, we applied percolation analysis [170] using a set of proportional thresholds (from 0.05 to 0.40 with 0.01 intervals) to identify the optimal sparsity level at which the largest component starts breaking apart (Figure 3.5, b).

Randomization of Networks

We generated 100 randomized networks based on the actual brain connectivity network for two key purposes: to calculate the small-worldness index (Figure 3.4) and to determine whether the value of Q significantly differed from the Q obtained by chance (Figure 3.8). For randomization, we started with the actual brain connectivity network and applied iterative rewiring using the Maslov and Sneppen [171] algorithm. Maslov-Sneppen rewiring is an efficient algorithm to sample random networks with the same number of nodes, connections, and node degree.

Small-worldness

Brain networks exhibit a small-world topology with high clustering, C, but low average minimum path length, L, compared to random networks. To quantify the "small-

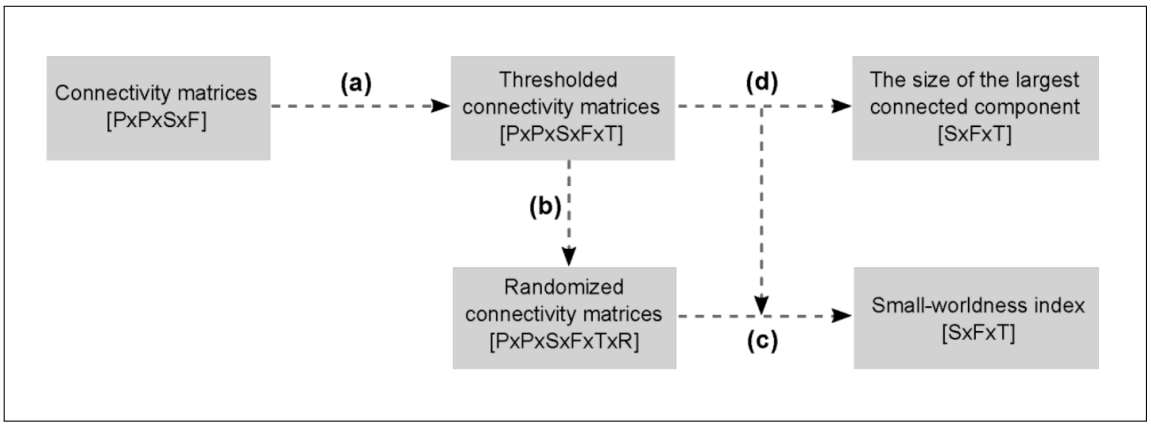

Figure 3.4 Connectivity matrices were thresholded at different sparsity levels (from 0.05 to 0.40 with 0.01 intervals) for each frequency band and each subject (a). Each thresholded matrix was used to generate 100 randomized networks (b). Randomized networks were used to calculate the small-worldness index (c). Percolation analysis was applied to the mean thresholded connectivity matrix to identify the sparsity level at which the largest connected component started breaking apart (d). $P = 400$ (parcels); $S = 96$ (subjects); $F = 3$ (frequency bands); $T = 5$ (proportional thresholds); $R = 100$ (randomizations).

worldness" of a network, Humphries and colleagues [172] proposed the Small-Worldness Index (σ), which is calculated as the ratio of normalized clustering (γ) to path length (λ). In small-world networks, where λ is approximately 1 and γ is greater than 1, the value of σ exceeds 1. A σ value greater than 1 indicates that the corresponding network exhibits small-world properties. At each sparsity level, a small-worldness index was calculated for each frequency band and each subject. Selected sparsity thresholds resulted in small-world networks as expected (Figure 3.5, a).

Percolation threshold

Bordier and colleagues showed that the percolation threshold maximizes information extracted by the community detection algorithm ([167]. Moreover, Nicolini's group revealed that the percolation analysis removes potentially spurious correlations and preserves the structure of functional connectivity networks [173]. We determined the largest connected component of the thresholded network via breadth-first search [174] at each sparsity level (Figure 3.5, b). Considering the small-worldness index and percolation analysis, we identified the optimum threshold as 30%.

Therefore, using percolation analysis, we identified the optimum sparsification

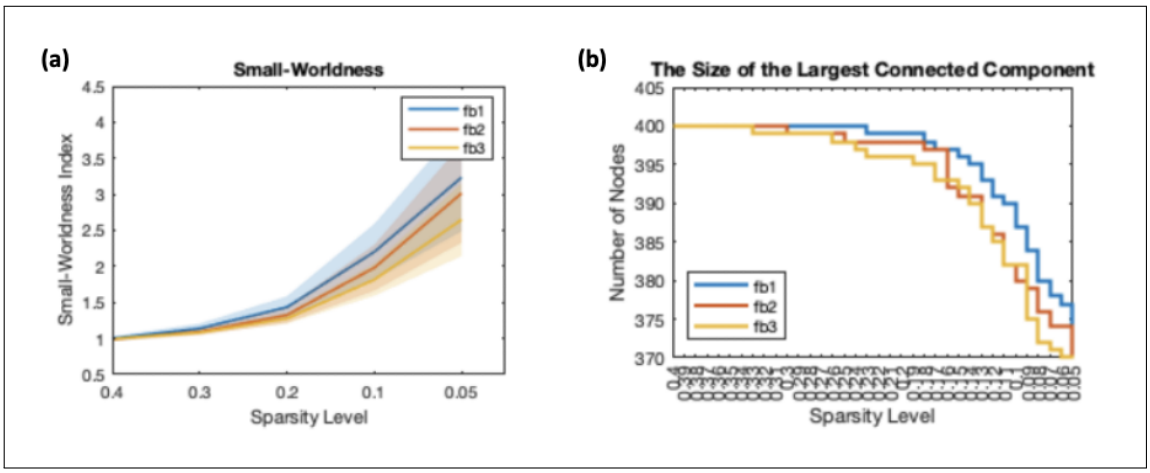

Figure 3.5 Therefore, using percolation analysis, we identified the optimum sparsification threshold as 30% and applied it to PC networks in further analysis.

threshold as 30% and applied it to PC networks in further analysis (Figure 3.4 and Figure 3.5).

3.4 Community Detection and Consensus Clustering

We ran a community detection algorithm called the "Louvain method" on PC matrices to detect functional brain modules [147]. The graph nodes represent parcels, and the edge weights indicate the phase consistency values between parcel pairs. The Louvain algorithm is based on an optimization that finds communities (groups of nodes) having denser connectivity with one another than is expected in a random null model. It yields a partition M indicating the module assignments of parcels and an index Q indicating the quality of modularity.

$$[Q, M] = \frac{1}{2W} \sum_{ij} \left(w_{ij} - \gamma e_{ij}^{w} \right) \delta(m_i, m_j) \tag{3.4}$$

where w_{ij} is the weight of the edge connecting node i and j, and $W = \frac{1}{2} \sum_{ij} w_{ij}$ is the total weight of edges of the network. The weight of edges linking nodes in the same community expected by chance is $e_{ij}^{w} = \frac{s_i s_j}{2W}$ where s_i and s_j are the sums of the

weights to nodes i and j, respectively. $\delta(m_i, m_j)$ is set to 1 when nodes are in the same community and 0 otherwise. Additionally, it has a tunable resolution parameter (γ) that defines the hierarchy (topological scale) in the modular organization. While low resolution reveals large communities, small communities become visible in high resolution.

The rationale behind the consensus clustering is based on the assumption that core nodes of network modules will be consistently grouped into the same community across different partitions. Therefore, consensus clustering reveals a representative community structure closest to the ground truth (Figure 3.4). We used the iterative consensus clustering algorithm (with the threshold $\tau = 0.1$ and 100 repetitions) proposed by Lancichinetti and Fortunato, which converges to a final representative partition [28].

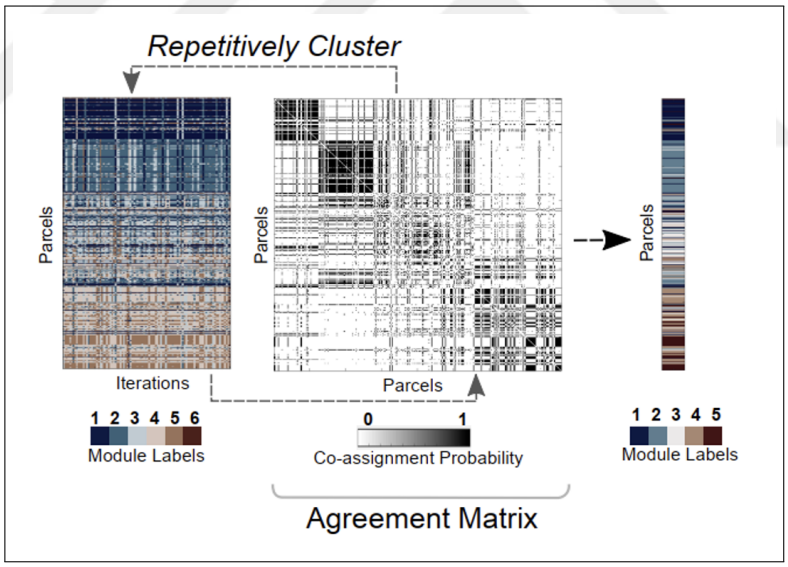

Figure 3.6 Consensus Clustering algorithm [27, 28].

Subject-Level Modular Decomposition: One of the critical issues in modularity analysis is to select the topological scale(s) of interest. Without prior knowledge, it is not easy to find a rationale for preferring one value of γ over another (including $\gamma = 1$). Selecting a single analysis scale is problematic, given that brain circuits exhibit hierarchically organized communities of various sizes across different topological scales. One approach to preserving brain community organization across multiple scales is consensus clustering across various spatial resolutions. Fenn et al. [175] suggested

that a "good" community structure should remain stable across a range of γ values. Therefore, we applied the Louvain algorithm on the phase-consistency matrices with resolution parameter γ changing between 0.1 and 2.9 in steps of 0.1. The Louvain algorithm is an optimization procedure which returns a slightly different result for every run. Therefore, we ran it 100 times for each γ value and applied consensus clustering over 100 iterations to find a representative subject-level modular decomposition for each γ [27, 28].

In order to identify the range of γ values that satisfy a stable community structure, which can further be compared with the widely investigated ICNs, we estimated the correspondence of our partitions with the 7 ICNs in the network atlas of Schaefer et al. [30] by computing the z-Rand index (z-score of the Rand similarity coefficient, Traud et al., 2011). A high z-Rand index is a statistical measure of the consistency between the two partitions in terms of whether two parcels fall into the same or different modules in each partition. As such, it reveals the matching of the two partitions independent of the topological scale, such that a cluster in a partition may correspond to a combination of clusters in the other partition. This criterion revealed a γ interval between 1 and 1.9 (Figure 3.7).

To capture the modular organization stable across the identified γ range, we applied consensus clustering over partitions obtained at each γ between 1 and 1.9. Therefore, using a 2-fold consensus clustering, we obtained a modular organization robust to algorithmic degeneracy and modular hierarchy. This final subject-level modular organization was used to investigate the node roles of brain regions.

Group-Level Modular Decomposition: The consensus clustering algorithm was run over subjects to find the modular organization common to all subjects. These modular structures that are robust to algorithmic degeneracy, hierarchy, and intersubject variability were used to define flexible regions.

Significance of Modularity

The modularity algorithm yields a positive Q value even for a non-modular network.

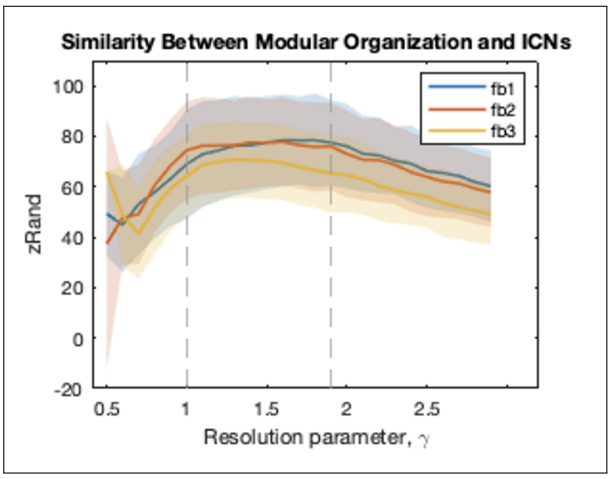

Figure 3.7 Similarity between Schaefer's parcels assigned to seven networks and the subject-level modular organization at each γ value. Shaded areas indicate the standard deviation of the mean over subjects. z-Rand has its maximum values in a range from 1 to 1.9.

Therefore, we tested the significance of Q by comparing it to a distribution obtained by 100 different randomized benchmark networks having the same number of nodes, weights, and strength distributions as the original. This permutation strategy tests against the null hypothesis that the observed modules are determined by chance (Figure 3.8 and Figure 4.1).

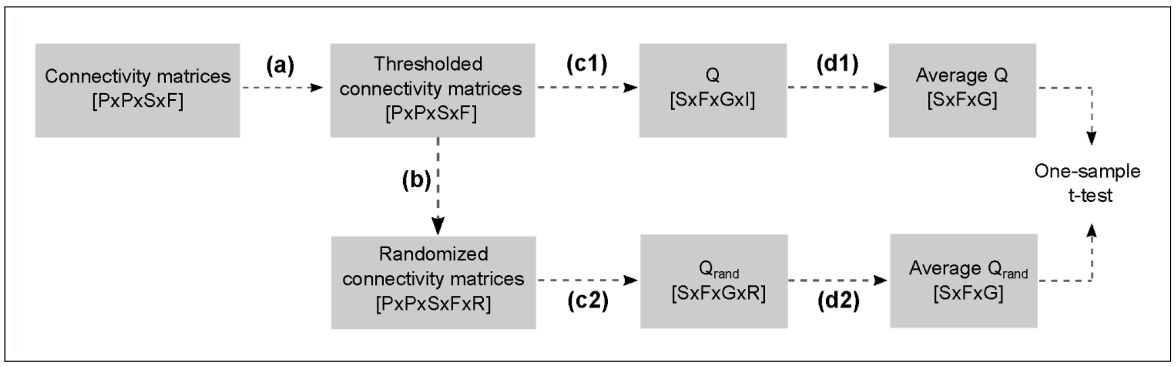

Figure 3.8 Connectivity matrices were thresholded at a sparsity level of 30% for each frequency band and each subject (a). Each thresholded matrix was randomized 100 times to generate null networks (b). The modularity algorithm using various γ values was applied 100 times to each $P \times P$ matrix to obtain Q values (c1). The modularity algorithm was applied to each $P \times P$ matrix using various γ values to obtain Q_{rand} values (c2). To test the difference between Q and Q_{rand} over subjects, we took the average over iterations for Q and randomizations for Q_{rand}. $P = 400$ (parcels); $S = 96$ (subjects); $F = 3$ (frequency bands); $R = 100$ (randomizations); $G = 29$ (γ values); $I = 100$ (iterations).

3.5 Integrative Regions

We used the flexibility of nodes to measure the modular assignment changes in the frequency domain (Figure 3.9). Flexibility, flex_i, is defined as the number of different modular assignments across frequency bands normalized by the total number of possible module assignments for node i [38].

$$\text{flex}_i = \frac{n}{N-1} \tag{3.5}$$

where n is the number of different modular assignments of node i across frequency bands and N is the number of frequency bands. It is important to keep in mind that module assignments in different frequency bands are simultaneous events. Brain regions assigned to the same module in all three frequency bands ($\text{flex}_i = 0$) are defined as "core" while regions with different module affiliations in different frequency bands ($\text{flex}_i > 0$) are defined as "flexible". These regions are called integrative regions as they have simultaneous intensive connections with different communities. Using a parcellation template assigning each parcel to an ICN helped us to understand the inter-network relations among the ICNs.

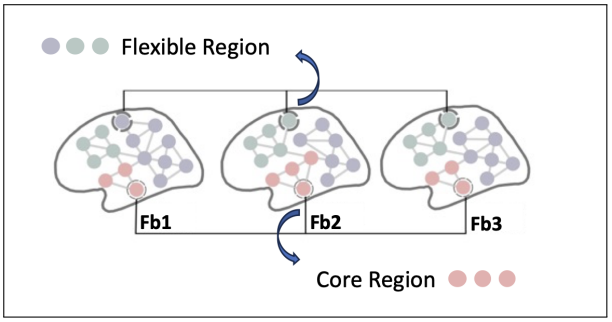

Figure 3.9 Flexibile and core regions.

3.6 Normalized Participation Coefficient

The participation coefficient P_i of node i measures the distribution of its connections across different modules and is defined as follows:

$$P_i = 1 - \sum_{m=1}^{M} \left(\frac{k_i(m)}{k_i} \right)^2 \tag{3.6}$$

where M is the number of modules in the network, $k_i(m)$ is the number of links between node i and other nodes in module m, and k_i is the degree between node i and all other nodes in the entire network (Figure 3.10) [35].

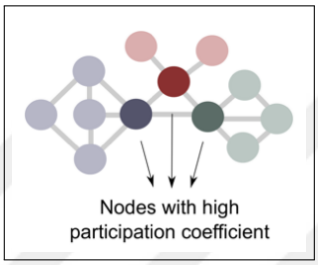

Figure 3.10 Figurative explanation of participation coefficient.

It has been shown that P_i is influenced by within-module connectivity, hence it may give biased results for networks with variable module sizes [176]. Therefore, we preferred to use the normalized participation coefficient P_i^{norm} that reduces the influence of within-network connectivity [177].

$$P_i^{\text{norm}} = 1 - \sqrt{B_0 \sum_{m=1}^{M} \left(\frac{k_i(m) - k_i(m)_{\text{rand}}}{k_i} \right)^2} \tag{3.7}$$

The key difference between P_i^{norm} and P_i is the involvement of the normalization factor, $k_i(m)_{\text{rand}}$, which is the median within-network degree for node i over 1000 randomized networks. The square rooting and a factor of $B_0 = 0.5$ ensure that the range is between 0 and 1. A weighted version of the normalized participation coefficient was computed for each node using subject-level modular organization.

3.7 Node Roles of Integrative Regions and Cognition

We have tested whether the P^{norm} values of integrative regions differed from those of the core regions with regard to their relation with high-order cognition. For each subject, we selected five cognitive domains of interest (two neuropsychological test scores for each domain) and fluid intelligence (Ravens Task score) for testing, listed in Table 3.7 [178].

Table 3.1
Behavioral data for fluid intelligence and five cognitive domains of interest (two test scores for each domain).

Description	**HCP Field**	**Cognitive Domain**
Fluid Intelligence (PMAT)	PMAT24_A_CR	Intelligence
Cognitive flexibility (DCCS)	CardSorting_AgeAdj	Executive Functions
Inhibition (Flanker task)	Flanker_AgeAdj	Executive Functions
Working Memory (List sorting)	ListSorting_AgeAdj	Working Memory
Processing Speed	ProcSpeed_AgeAdj	Working Memory
Vocabulary (picture matching)	PicVocab_AgeAdj	Language
Reading (pronunciation)	Reading	Language
Visual Episodic Memory	Pic_Seq_AgeAdj	Memory
Verbal Episodic Memory	IWRD_TOT	Memory
Visuospatial orientation	VSPLOT_TC	Visuospatial
Visuospatial orientation	VSPLOT_OFF	Visuospatial

PMAT: Penn Progressive Matrices; *DCCS*: Dimensional Change Card Sort.

3.8 Statistical Analysis

We formulated a multiple linear regression model with $N_{\text{peri}} + N_{\text{core}}$ independent variables as follows:

$$Y = X\beta + \epsilon \tag{3.8}$$

where $Y \in R^{N_{\text{sub}} \times N_{\text{behav}}}$ was the behavioral data, $X = [1\, F\, C]$, $X \in R^{N_{\text{sub}} \times (1+N_{\text{peri}} \times N_{\text{core}})}$ was the design matrix whose rows contained the P^{norm} values of an attention network for subjects. 1 represents a column vector consisting of ones accounting for the constant effect, F and C matrices contain the P^{norm} values of each flexible region and core region as columns, respectively. $\beta \in R^{(1+N_{\text{peri}} \times N_{\text{core}}) \times N_{\text{behav}}}$ was the associated matrix of linear regression parameters relating the P^{norm} values to behavioral data. For each behavior measure $y_i \in R^{N_{\text{sub}} \times 1}$, we performed a t-test with a significance level of 0.05 on estimated coefficients ($\hat{\beta}$) to check for any difference between the regression parameters for the peripheral and core regions. For each column of β corresponding to a particular behavioral data, the t-statistics were computed as

$$t_{N_{\text{sub}}-(N_{\text{peri}}+N_{\text{core}}+1)} \sim \frac{c^T \hat{\beta}}{\sqrt{\hat{\sigma}^2 c^T (X^T X)^{-1} c}} \tag{3.9}$$

where $c = [0\, 1\, 1 \ldots 1\ -1\ -1 \ldots -1]$ is a contrast vector differencing the sum of peripheral and core regions' parameters. $\hat{\beta} = (X^T X)^{-1} X^T Y$ represents the estimated regression parameters, $\hat{\sigma}^2 = \text{std}(RY)$ is the standard deviation of the residual error, and $\epsilon = Y - X\hat{\beta} = (I - (X^T X)^{-1} X^T)Y = RY$ is the error.

An important assumption for the general linear model was that the residuals were normally distributed. So, we used a Q-Q (quantile-quantile) plot to check whether our residuals were normally distributed. To assess statistical significance, we performed a permutation test where we shuffled the assignments of the parcels (integrative or core) in X, refitted the model, and repeated the procedure 10,000 times. This process led to an empirical null distribution of t-values for each behavioral measure. Then, we computed the p-values for each test. Permutation-based t-tests were performed for each ICN of interest and for P^{norm}. The estimated p-values were adjusted for multiple comparisons using the false discovery rate (FDR) approach with a significance level of

$\alpha = 0.05$.

Software and Code

The analyses were conducted using MATLAB 2022a (MathWorks Inc., MA, USA). Codes for graph metrics were used from the Network Community Toolbox (http://commdetect.weebly.com) and the Brain Connectivity Toolbox [24] (https://sites.google.com/site/bctnet/Home).

4. RESULTS

4.1 Three Main Modules and Corresponding ICNs

For subject-level modular organization, we have tested the significance of Q with respect to its null distribution derived from randomized networks ($N = 100$) having the same number of nodes, weights, and strength distributions as the empirical connectivity network. We showed that observed Q values were significantly higher than Q values obtained by chance ($P < 0.001$, Figure 4.1).

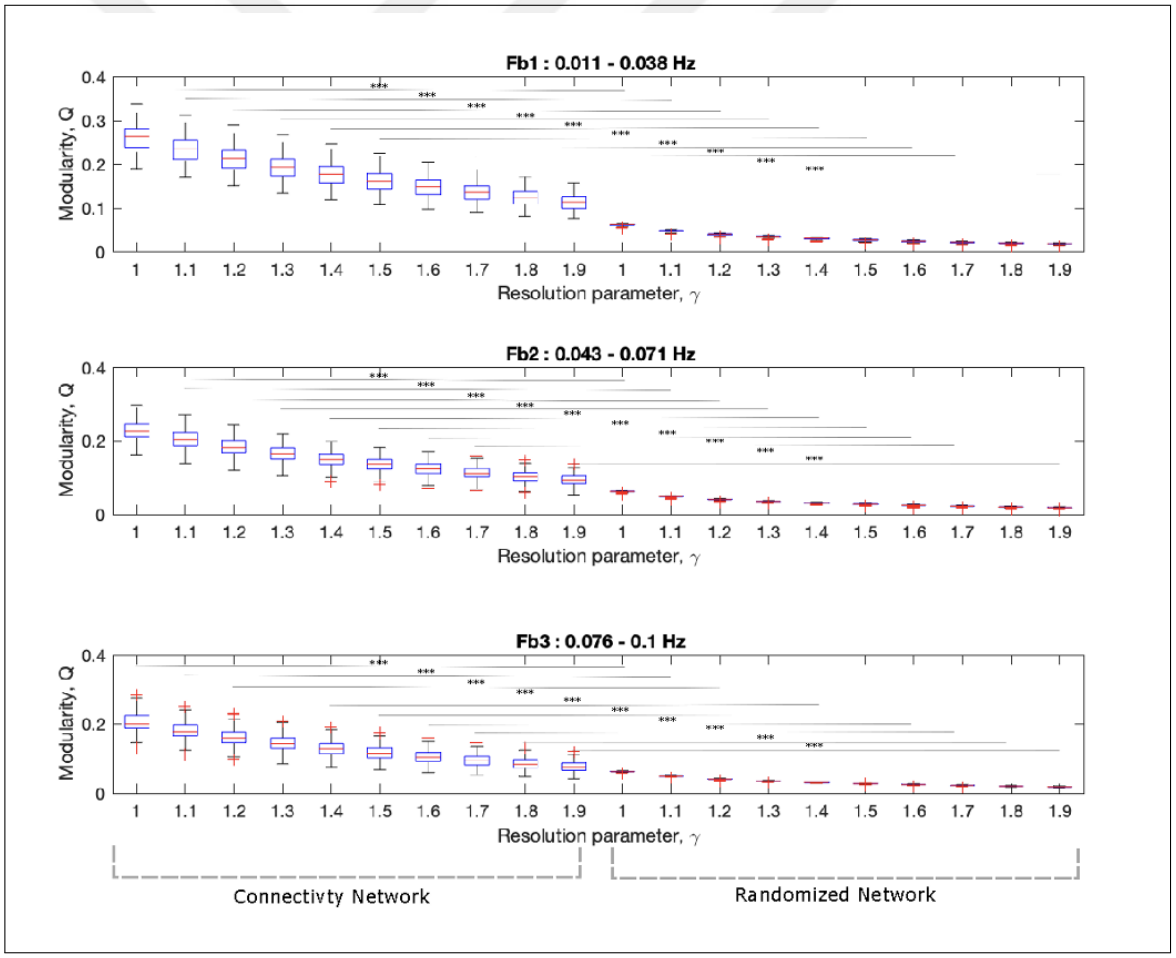

Figure 4.1 We performed a one-sample t-test over subjects to determine whether that difference was significantly greater than or less than zero for each γ value. Boxplots show the modularity index Q in the brain network compared to randomized networks (Q_{rand}). Error bars indicate the standard deviation in the mean over subjects. *** indicates that $p_{\text{fdr}} < 0.001$ for the one-sample t-test where p_{fdr} stands for the FDR-corrected p-value.

Three main modules were obtained, which corresponded to a module covering the VN and parts of the DAN, a second cognitive module that covered the DMN, LN, ECN and parts of the two attention networks, SN/VAN and DAN, and a third containing the SMN and parts of the SN/VAN (Figure 4.2).

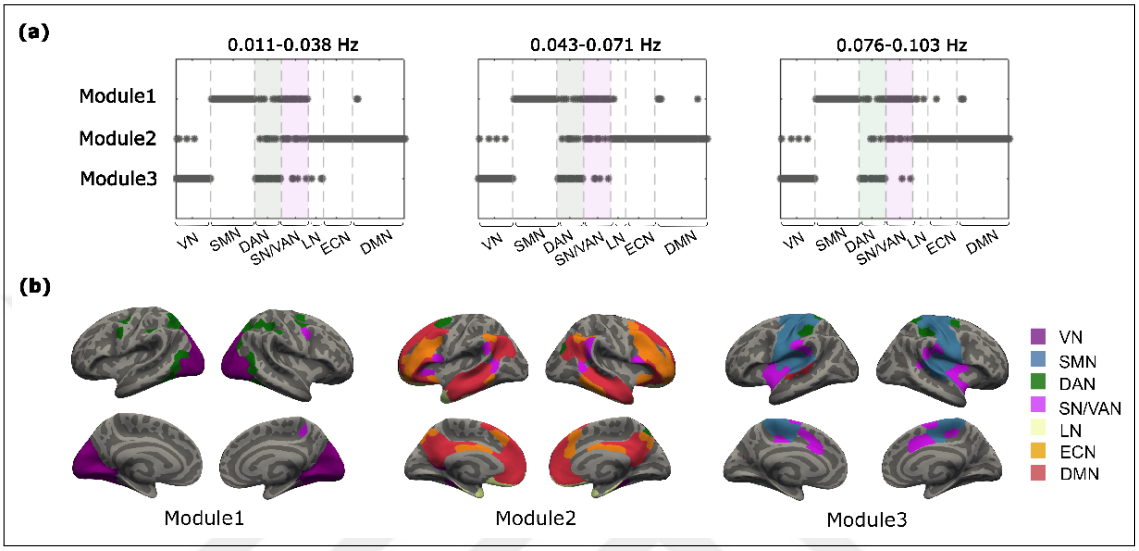

Figure 4.2 Three main modules were revealed via group-level analysis. Module 1 covers the VN and parts of the DAN, Module 2 covers the DMN, ECN, and LN, and Module 3 contains the SMN and parts of the SN/VAN. Dots identify the module assignment of each parcel. Parcels belonging to attention networks are distributed among these three modules. Shaded areas correspond to attention networks (a). Core parcels assigned to the same module in all three frequency bands are represented on the cortex (VN, visual network; DAN, dorsal attention network; DMN, default mode network; ECN, executive control network; LN, limbic network; SMN, somatomotor network; SN/VAN, salience/ventral attention network) (b).

4.2 Core and Integrative Regions

Parcels with $\text{flex}_i = 0$ were called core regions and remained in one of the main modules across three frequency bands. As shown in Figure 4.3, the majority of the parcels are in the core. On the other hand, there were some flexible regions, which we called integrative regions, that were distributed over five different ICNs. However, almost 70% of them were in the attention networks (Figure 4.3).

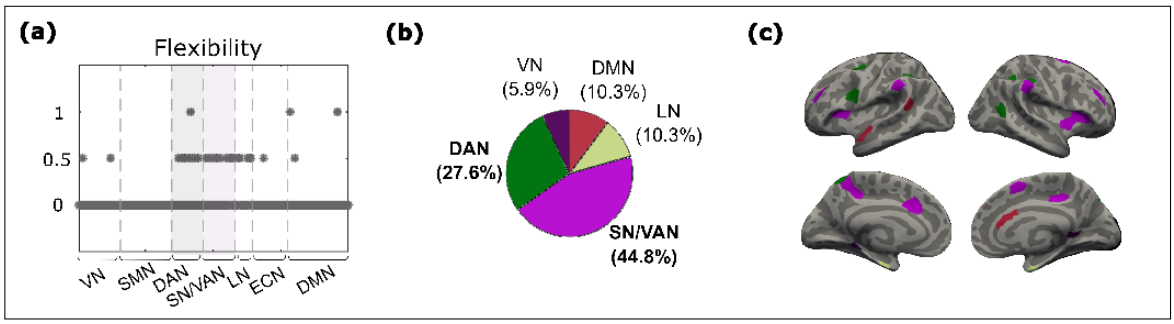

Figure 4.3 Core Regions on Attention Networks.

4.3 Core Regions on Attention Networks

It was observed that 72% of the nodes (34/47) in the SN/VAN fell into the same module in all three frequency bands (Figure 4.4). These core regions in the SN/VAN were distributed over the three main components of the network and usually had dense connections with the SMN-centered (Module 3) and cognitive (Module 2) modules (Fig. 6a). Similarly, 83% of the nodes in DAN were densely connected to VN-centered (Module 1) and cognitive (Module 2) modules consistently in three frequency bands.

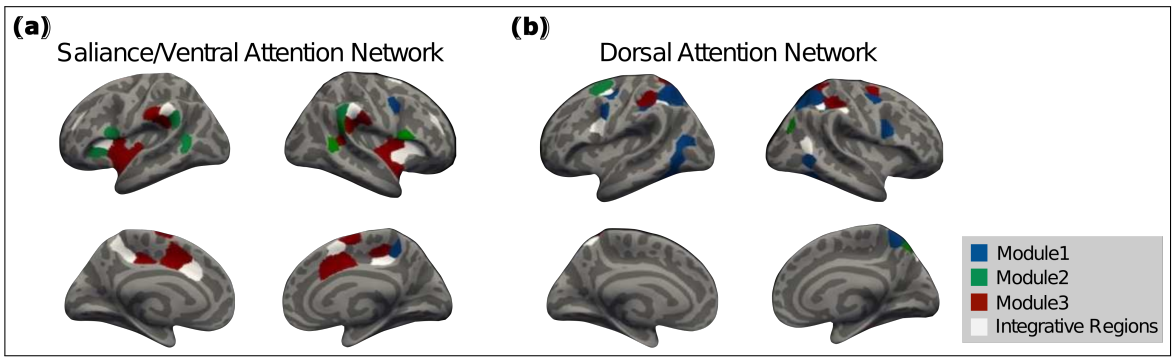

Figure 4.4 Core and integrative regions within the attention networks. White parcels are the integrative regions, while core regions are color-coded. Module1, Module2, and Module3 are dominated by VN, DMN, and SMN, respectively. VN, visual network; DMN, default mode network; SMN, somatomotor network.

4.4 Integrative Regions on Attention Networks

When the nodes were investigated, it was observed that 28% in the SN/VAN and 17% in the DAN were behaving as integrative regions. Integrative regions in the

SN/VAN mainly had dense connections with the SMN-centered and cognitive modules. More specifically, 11 out of the 13 integrative nodes of the SN/VAN participated in the cognitive module in a relatively low-frequency band (0.011-0.038 Hz) and the SMN-centered module in a higher frequency band (0.043-0.071 Hz). On the other hand, integrative regions in the DAN had dense connections with the VN-centered and cognitive modules. In this case, five out of the eight integrative nodes of the DAN participated in the cognitive module in a relatively low-frequency band (0.043-0.071 Hz) and the VN-centered module in a higher frequency band (0.076-0.103 Hz). In general, integrative regions in attention networks preferred higher-level cognitive networks in relatively lower frequencies and sensory-motor networks in relatively higher frequencies (Figure 4.5).

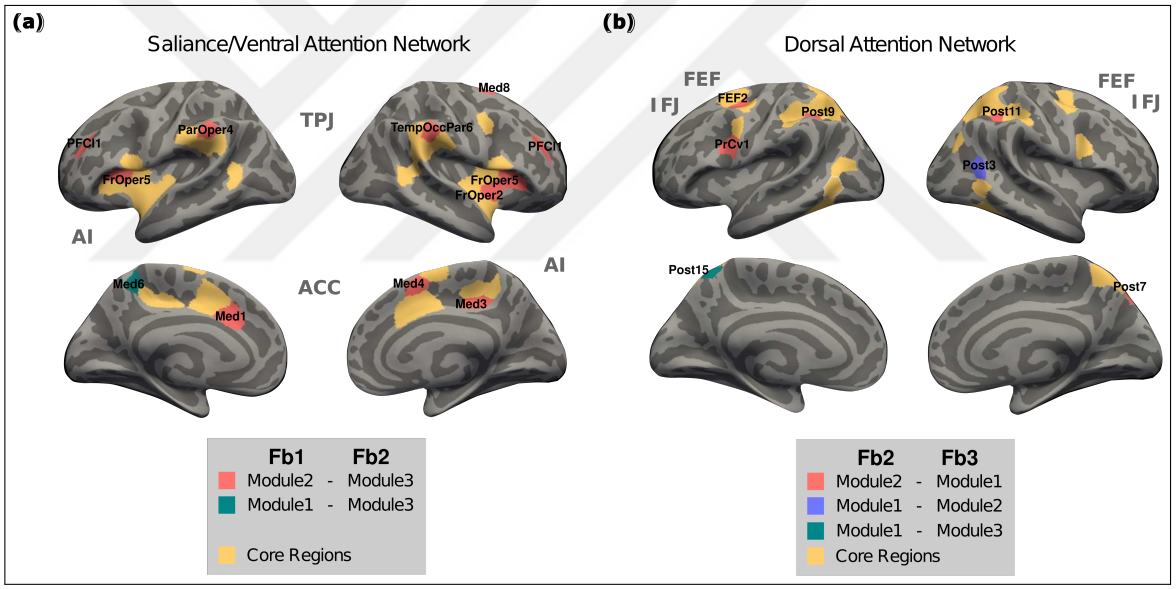

Figure 4.5 Frequency selective module participation of integrative regions in attention networks. Integrative regions participate in the cognitive module at a frequency band and in either one of the visual or somatomotor modules in another frequency band. Yellow indicates the core parcels. Modular assignments of integrative regions in different frequency bands were color-coded. Module1, CN-centred; Module2, Cognitive; Module3, SMN-centred. VN, visual network; DMN, default mode network; SMN, somatomotor network; TPJ, temporoparietal junction; AI, anterior insula; ACC, anterior cingulate cortex; FEF, frontal eye field; IFJ, inferior frontal junction.

4.5 Node Roles of Integrative Regions and Cognition

The results of the permutation-based t-test investigating whether the P^{norm} values of integrative regions differed from those of the core regions due to their relation to higher-order cognition are presented in Table 4.1.

Table 4.1
Significant results of permutation-based t-tests showed that the P^{norm} of integrative regions differed from the core regions regarding their relation with high-order cognition such as intelligence, executive functions, and working memory.

HCP Field	**Cognitive Domain**	**SN/VAN** t	**SN/VAN** p_{fdr}	**DAN** t	**DAN** p_{fdr}
PMAT24_A_CR	Intelligence	-1.47	0.891	2.72	0.016*
CardSorting_AgeAdj	Executive Functions	3.42	0.018*	0.64	0.302
Flanker_AgeAdj	Executive Functions	1.67	0.115	1.02	0.302
ListSorting_AgeAdj	Working Memory	2.60	0.032*	1.45	0.335
ProcSpeed_AgeAdj	Working Memory	3.18	0.032*	0.19	0.430
PicVocab_AgeAdj	Language	-0.10	0.615	0.58	0.419
Reading	Language	-0.29	0.615	0.19	0.419
Pic_Seq_AgeAdj	Memory	1.76	0.194	-0.65	0.911
IWRD_TOT	Memory	1.26	0.194	-1.03	0.911
VSPLOT_TC	Visuospatial	0.52	0.669	-1.37	0.848
VSPLOT_OFF	Visuospatial	-0.61	0.669	0.46	0.752

*S*N/VAN, salience/ventral attention; DAN, dorsal attention network. p_{fdr} represents p-values corrected using the false discovery rate method with respect to cognitive domains. * Indicates $p_{\text{fdr}} < 0.05$.

For SN/VAN, results indicated significant differences between integrative and core regions when their P^{norm} values were related to three cognitive tasks in two cognitive domains: executive function and working memory. For DAN, correlations between P^{norm} values of integrative regions and intelligence scores were significantly stronger than those of core regions.

5. DISCUSSION

We focused deliberately on the conventional frequency range (0.01 and 0.1 Hz) of most fMRI studies to be able to discuss our results with existing reports. Since there is no commonly accepted convention for frequency sub-band splitting of the BOLD signal, we preferred to divide the frequency range into three sub-bands of equal width which roughly overlapped with the frequency limits of the slow-3 (0.073-0.198 Hz), slow-4 (0.027-0.073 Hz), and slow-5 (0.01-0.027 Hz) frequency bands investigated in previous fMRI studies [121] Yang et al., 2022). These previous fMRI works referred their sub-band selection to the ultra-slow frequency bands observed in electrophysiological studies [16,179]. In addition to the overlapping frequency range of the BOLD signal with ultra-slow electrophysiological oscillations, the presence of significant correlations between the ongoing BOLD amplitudes and the amplitude envelopes of various higher-frequency EEG rhythms in delta, theta, alpha, beta, or gamma bands [18, 180] further suggests that various frequency sub-bands of the BOLD may have special biological meanings in parallel to those in electrophysiological recordings [16].

The group-level modularity analyses based on phase consistency revealed three large modules, which were consistent over the three frequency bands. In accordance with the literature [181], three main modules were a VN-centered, an SN-centered, and a cognitive module covering LN, ECN, and DMN. The two attention networks, SN/VAN and DAN, were distributed among these three main modules. Some of the studies focusing on different levels of modular hierarchy revealed more than three modules [182]. However, we consider that the phase-consistency-based functional connectivity metric provides insight about a higher-level modular organization with a lesser number of overarching modules, which is shortly discussed under the next subheading.

5.1 Is the Correlation Coefficient-Based Functional Connectivity Sufficient to Reveal the Network Dynamics?

Phase difference around 180 degrees would yield a strong negative Pearson's correlation coefficient (CC) value, distinct from a similarly strong positive one around 0 phase lag. Such negative correlations are usually interpreted as counter-connectivity or reciprocal suppression of two brain regions and evaluated as a critical distinction criterion for task-negative and task-positive networks. On the other hand, CC would be zero in a case when a 90-degree phase difference between two signals occurs, even though the two time series would be strongly coherent [183].

Although the neurophysiological validity and the role of BOLD anticorrelation [184] in the hierarchy among ICNs have been advocated, it bears some limitations. The BOLD signal does not provide a direct distinction between the excitatory or inhibitory activities since it reflects the metabolic activity of a neuronal population. Hence, increased BOLD in a specific area may correspond to either an increased excitation or inhibition, and reduced BOLD to a reduced excitation or inhibition in an area. Therefore, the positivity or negativity of the correlations between the BOLD signals in two brain areas provides a partial view of whether they activate or inhibit each other. We assume that using an FC metric that represents the strength of the connection independent of any phase delay might complement and extend our understanding of the modular organization of the brain.

Instead of the conventional correlation coefficient, we used the consistency of the phase differences between BOLD signals so that their strength of association was determined by the similarity of the phase differences rather than the phase differences themselves. In this way, instead of two distinct modules, such as "task-positive" ECN and task-negative "DMN," we obtained a single cognitive module that contained both ICNs due to the fact that the phase consistency metric was insensitive to phase delays around 180 degrees. Furthermore, in line with our expectation, most of the flexible nodes turned out to be in attention networks, especially in SN/VAN as one striking

observation in our study. Overall, these results may shed light on the mechanism underlying the hierarchical modular organization of the brain.

5.2 Can Frequency Characteristics of the BOLD Signal be Significant in Estimating the Network Dynamics?

The correlation coefficients computed over the wide-band signal provide only information about the part of the frequency band dominating the spectrum therby masking the contribution from the frequency range with relatively lower power. By separately evaluating the different frequency sub-bands, the frequency-domain phase-based connectivity metric avoids such bias and can measure the coherence in low amplitude frequency components as well.

The frequency dependency of the within and between network functional connectivity in fMRI has already been tested in a series of studies [19, 121, 126]. These studies either used exploratory frequency bands [45, 185–187] or attempted to identify particular frequency ranges by investigating the coherence spectra of brain regions [125], searching for the peaks of small-worldness network property [126], or evaluating the ICN efficiency [127]. As a result, Sasai and coworkers [125] and Thompson and Fransson [126] showed differences in within- and between-network connectivity with respect to frequency. Wu's group [19] further claimed that cortical ICNs concentrated on the ultra-low frequency range (0.01-0.06 Hz), while subcortical limbic networks were distributed over a wider frequency range (0.01-0.14 Hz). These observations on the significance of various frequency sub-bands of the BOLD signal support our working hypothesis on the interaction of the same node with different modules using different frequency channels.

5.3 Intermediate Position of the Two Attention Networks Between the Sensory-Motor and Cognitive Networks

Most of the frequency-dependent flexibility was associated with two attention networks (SN/VAN, DAN). From a functional point of view, the intermodular position of the attention networks among these three modules is strongly plausible, as they act on peripheral sensory inputs and motor outputs by integrating them with motivational and memory-related aspects processed by higher-level cognitive networks. Covering the somatic sensory and auditory sensory areas and motor cortices, 11 of the 13 flexible SN/VAN regions were coherent with the cognitive module in a lower and with the SMN in a higher frequency range. Additionally, five out of the eight flexible DAN nodes were interacting with the VN in a higher frequency range in addition to their simultaneous positions within the cognitive module in a lower frequency band. The general frequency characteristics of these nodes showing integration with sensory-motor areas in a higher frequency range in contrast to their interaction with the cognitive module in a lower frequency range are in agreement with the reported results on EEG [188].

5.4 Flexibility of the Attention Networks

It has been reported in several studies that the SN offers remarkably rapid responses to external and internal salient events, including errors, and accordingly regulates the interaction between the DMN and the ECN. As the cognitive burden increases, SN switches the control from DMN to ECN by reducing the intrinsic connectivity of the DMN but increasing that of the ECN. Therefore, dynamic interactions between SN, DMN, and ECN seem to play a crucial role in cognitive functions. In line with this, Chen and coworkers suggest that the SN has the highest level of flexibility in time-varying connectivity compared to other networks.

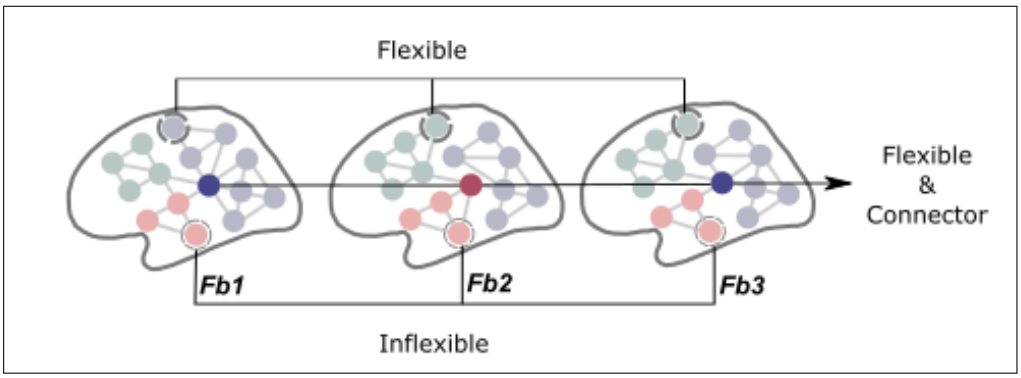

Figure 5.1 Flexible nodes with connector role.

5.5 Flexible Node-Specific Regression Patterns with Cognitive Test Scores

In line with the characteristics of the SN and the intermediate position of the VAN and DAN between sensory-motor and cognitive modules, we found most of the frequency-domain flexible nodes in areas assigned to SN/VAN and DAN. The modular assignment of these nodes to one of the SMN or VN networks while simultaneously communicating with the cognitive module points to their importance in the integration of the sensory inputs and motor outputs with the intrinsic cognitive state of the brain. The higher regression parameters of the normalized participation coefficients (P^{norm}) of these flexible regions with the executive functions, working memory, and intelligence scores support the evidence for their integrative role in contrast to those of the core regions.

5.6 Limitations

We focused on the frequency bands corresponding to the conventional frequency range of 0.01-0.1 Hz to obtain results comparable to the existing literature. However, it can be considered a limitation of the present study since convincing results for meaningful neural content at frequencies higher than 0.1 Hz, even up to 0.75 Hz, have also been reported. In a future study, we plan to extend the frequency range and investigate the frequency selectivity of integrative regions in a broader frequency range.

In this study, we analyzed resting-state fMRI data and investigated its relation to the cognitive test scores of subjects. In the future, applying a similar approach to task-based fMRI data can help to study the direct relationship between the BOLD signal and behavior.

6. CONCLUSION

The contributions of this study are threefold. First, the frequency-domain analysis of the BOLD coherences among brain regions reveals specific areas that may play a role in the inter-modular integration by simultaneous engagement with different brain modules in different frequency ranges due to functional flexibility. Second, most of these flexible regions reside in attention networks and communicate with higher-order cognitive cortices in a relatively lower frequency band while they interact with the sensory and motor areas in higher frequency bands. Hence, these attention network areas may play a strong integrative role at the intermediate level between the sensory/motor and high-order cognitive networks. Such integration capacity is also observed as a stronger relation between the P^{norm} values of the flexible regions and relevant neuropsychological test scores, which is weaker in the core nodes. Lastly, these results emphasize the importance of analyzing BOLD signals in narrower frequency bands to reveal hidden dynamics that traditional whole-band analyses might overlook. Considering the wealth of frequency-domain findings in brain electrophysiological studies, more refined time-frequency analyses may provide new opportunities to discover functionally important features of the BOLD dynamics.

These contributions underline the necessity of adopting a frequency-specific approach to better understand brain network dynamics. Furthermore, the results have potential implications for clinical neuroscience, where identifying frequency-specific changes may enhance our understanding of neurological and psychiatric conditions and inform interventions targeting cognitive and behavioral disorders. Future research should aim to extend these findings by integrating multimodal neuroimaging data and exploring dynamic frequency-domain flexibility under task-based conditions.

APPENDIX A. PUBLICATIONS

First author

1. Neşe, H., Harı, E., Ay, U., Demiralp, T., & Ademoğlu, A. (2024). Integrative role of attention networks in frequency-dependent modular organization of human brain. Brain Structure and Function, 1-13.

Coauthor

1. Harı, E., Ay, U., Neşe, H., Bayram, A., & Demiralp, T. (2020). Manyetik Rezonans Görüntüleme Temelli Fonksiyonel Bağlantısallık Yöntemleri. Journal of Istanbul Faculty of Medicine, 83(1), 71-80.

International Conference Proceedings and Abstracts

First author

1. Neşe, E., Ademoğlu, A., & Demiralp, T. (2024). Frequency-Dependent Dynamics of Intrinsic Connectivity Networks: A Multilayer Analysis of BOLD Signals. European Society for Magnetic Resonance in Medicine and Biology (ESMRMB24). (Oral presentation)
2. Neşe, E., Ademoğlu, A., & Demiralp, T. (2024). Integrative Role of Attention Networks in Multi-Frequency Modular Organization of Human. Brain Organization for Human Brain Mapping (OHBM). (Poster)
3. Neşe, E., Ademoğlu, A., & Demiralp, T. (2024). Frequency-varying modular organization in resting-state fMRI. 1. Ulusal Nörogörüntüleme Kongresi & 2nd Joint German-Turkish Symposium On Human Neuroscience. (Oral presentation)
4. Neşe, H., Ademoğlu, A., & Demiralp, T. (2023).Frequency-varying Organization of Resting StateFunctional Connectivity.European Neuroscience Conference by Doctoral Students (ENCODS23). (Oral presentation)
5. Neşe, H.,Harı, E., Ademoğlu, A., & Demiralp, T. (2022). Phase-Consistency Based Frequency-Domain Analysis of Brain Network Modularity. Organization for Human Brain Mapping (OHBM). (Poster)

6. Neşe, H., Ademoğlu, A.Bayram, A., Demiralp, T.(2019). Evaluating the Cross-Frequency Coupling of Restand Task fMRI Signal. European Neuroscience Conference for Doctoral Students(ENCODS), London, United Kingdom. (Poster)
7. Neşe, H., Soylu, C., Irak, M., Adanalı, P., & Akın, A. (2015) Functional Connectivity of Resting State as a Biomarker for Working Memory Performance. (Poster)

National Conference Proceedings and Abstracts

First author

1. Neşe, H. FMRI'da çok bantlı analizler: İçsel bağlantı ağlarının frekansa bağlı dinamikleri. Ulusal Sinibilim Kongresi (USK24) (Panel talk)
2. Neşe, H., Ademoğlu, A., & Demiralp, T. (2022). The integrative position of attention networks between cognitive, sensory and motor modules.Anatomy: International Journal of Experimental & Clinical Anatomy, 16. (oral presentation)
3. Neşe, H.,Bayram, A., Har i, E., Kurt, E., Ademoğlu, A., & Demiralp, T. (2021, June). Phase consistency analysis of the brain functional connectivity networks. 29th Signal Processing and Communications Applications Conference (SIU)(pp.1-4). IEEE. (Oral presentation)
4. Neşe, H., Bayram, A., Demiralp, T., & Ademoğlu, A. (2020). Spatial synchronization patterns within intrinsic connectivity networks in resting-state fMRI.Anatomy: International Journal of Experimental &Clinical Anatomy,14. (Oral presentation)

Coauthor

1. Soylu C., Kıçik A., Bayram A.,Neşe H., Gürvit İ.H., Demiralp T.(2022).Investigation of functional connectivity network in Parkinson's disease with machine learning methods.Anatomy: International Journal of Experimental & Clinical Anatomy, 16

REFERENCES

1. Sporns, O., "Network attributes for segregation and integration in the human brain," *Current Opinion in Neurobiology*, Vol. 23, no. 2, pp. 162–171, 2013.

2. Wernicke, C., *Der aphasische Symptomencomplex: eine psychologische Studie auf anatomischer Basis*, Cohn & Weigert, 1874.

3. Lichtheim, L., "On aphasia," *Brain/Oxford*, 1885.

4. Geschwind, N., "The organization of language and the brain: Language disorders after brain damage help in elucidating the neural basis of verbal behavior.," *Science*, Vol. 170, no. 3961, pp. 940–944, 1970.

5. Chang, E. F., Raygor, K. P., and Berger, M. S., "Contemporary model of language organization: an overview for neurosurgeons," *Journal of Neurosurgery*, Vol. 122, no. 2, pp. 250–261, 2015.

6. Mesulam, M.-M., "From sensation to cognition.," *Brain: A Journal of Neurology*, Vol. 121, no. 6, pp. 1013–1052, 1998.

7. Biswal, B., *et al.*, "Functional connectivity in the motor cortex of resting human brain using echo-planar mri," *Magnetic Resonance in Medicine*, Vol. 34, no. 4, pp. 537–541, 1995.

8. Raichle, M. E., *et al.*, "A default mode of brain function," *Proceedings of the National Academy of Sciences*, Vol. 98, no. 2, pp. 676–682, 2001.

9. Fox, M. D., *et al.*, "The human brain is intrinsically organized into dynamic, anticorrelated functional networks," *Proceedings of the National Academy of Sciences*, Vol. 102, no. 27, pp. 9673–9678, 2005.

10. Corbetta, M., and Shulman, G. L., "Control of goal-directed and stimulus-driven attention in the brain," *Nature Reviews Neuroscience*, Vol. 3, no. 3, pp. 201–215, 2002.

11. Dosenbach, N. U., *et al.*, "Distinct brain networks for adaptive and stable task control in humans," *Proceedings of the National Academy of Sciences*, Vol. 104, no. 26, pp. 11073–11078, 2007.

12. Power, J. D., *et al.*, "Functional network organization of the human brain," *Neuron*, Vol. 72, no. 4, pp. 665–678, 2011.

13. Petersen, S. E., and Posner, M. I., "The attention system of the human brain: 20 years after," *Annual Review of Neuroscience*, Vol. 35, no. 1, pp. 73–89, 2012.

14. Buckner, R. L., Krienen, F. M., and Yeo, B. T., "Opportunities and limitations of intrinsic functional connectivity mri," *Nature Neuroscience*, Vol. 16, no. 7, pp. 832–837, 2013.

15. Margulies, D. S., *et al.*, "Situating the default-mode network along a principal gradient of macroscale cortical organization," *Proceedings of the National Academy of Sciences*, Vol. 113, no. 44, pp. 12574–12579, 2016.

16. Buzsáki, G., and Draguhn, A., "Neuronal oscillations in cortical networks," *Science*, Vol. 304, no. 5679, pp. 1926–1929, 2004.

17. Buzsáki, G., Logothetis, N., and Singer, W., "Scaling brain size, keeping timing: evolutionary preservation of brain rhythms," *Neuron*, Vol. 80, no. 3, pp. 751–764, 2013.

18. Mantini, D., *et al.*, "Electrophysiological signatures of resting state networks in the human brain," *Proceedings of the National Academy of Sciences*, Vol. 104, no. 32, pp. 13170–13175, 2007.

19. Wu, C. W., *et al.*, "Frequency specificity of functional connectivity in brain networks," *Neuroimage*, Vol. 42, no. 3, pp. 1047–1055, 2008.

20. De Domenico, M., Sasai, S., and Arenas, A., "Mapping multiplex hubs in human functional brain networks," *Frontiers in Neuroscience*, Vol. 10, p. 326, 2016.

21. Barabási, A.-L., *Network Science*, Cambridge, UK: Cambridge University Press, 2018.

22. Euler, L., "Solutio problematis ad geometriam situs pertinentis," *Commentarii Academiae Scientiarum Imperialis Petropolitanae*, Vol. 8, pp. 128–140, 1736.

23. Bryce, N. V., *et al.*, "Brain parcellation selection: An overlooked decision point with meaningful effects on individual differences in resting-state functional connectivity," *NeuroImage*, Vol. 243, p. 118487, 2021.

24. Rubinov, M., and Sporns, O., "Complex network measures of brain connectivity: uses and interpretations," *Neuroimage*, Vol. 52, no. 3, pp. 1059–1069, 2010.

25. Shenoy Handiru, V., *et al.*, "Graphâtheoretical analysis of eeg functional connectivity during balance perturbation in traumatic brain injury: A pilot study," *Human Brain Mapping*, Vol. 42, no. 14, pp. 4427–4447, 2021.

26. Fornito, A., Zalesky, A., and Bullmore, E., "Fundamentals of brain network analysis academic press.[google scholar]," 2016.

27. Betzel, R. F., "Community detection in network neuroscience," in *Connectome Analysis*, pp. 149–171, Academic Press, 2023.

28. Lancichinetti, A., and Fortunato, S., "Consensus clustering in complex networks," *Scientific Reports*, Vol. 2, no. 1, p. 336, 2012.

29. Yin, D., and Kaiser, M., "Understanding neural flexibility from a multifaceted definition," *NeuroImage*, Vol. 235, p. 118027, 2021.

30. Schaefer, A., *et al.*, "Local-global parcellation of the human cerebral cortex from intrinsic functional connectivity mri," *Cerebral Cortex*, Vol. 28, no. 9, pp. 3095–3114, 2018.

31. Cohen, J. R., and D'Esposito, M., "The segregation and integration of distinct brain networks and their relationship to cognition," *Journal of Neuroscience*, Vol. 36, no. 48, pp. 12083–12094, 2016.

32. Fox, M. D., and Raichle, M. E., "Spontaneous fluctuations in brain activity observed with functional magnetic resonance imaging," *Nature Reviews Neuroscience*, Vol. 8, no. 9, pp. 700–711, 2007.

33. Yeo, B. T., *et al.*, "The organization of the human cerebral cortex estimated by intrinsic functional connectivity," *Journal of Neurophysiology*, 2011.

34. Sporns, O., and Betzel, R. F., "Modular brain networks," *Annual Review of Psychology*, Vol. 67, no. 1, pp. 613–640, 2016.

35. Guimera, R., and Amaral, L. A. N., "Cartography of complex networks: modules and universal roles," *Journal of Statistical Mechanics: Theory and Experiment*, Vol. 2005, no. 02, p. P02001, 2005.

36. Preti, M. G., Bolton, T. A., and Van De Ville, D., "The dynamic functional connectome: State-of-the-art and perspectives," *Neuroimage*, Vol. 160, pp. 41–54, 2017.

37. Betzel, R. F., and Bassett, D. S., "Multi-scale brain networks," *Neuroimage*, Vol. 160, pp. 73–83, 2017.

38. Bassett, D. S., *et al.*, "Dynamic reconfiguration of human brain networks during learning," *Proceedings of the National Academy of Sciences*, Vol. 108, no. 18, pp. 7641–7646, 2011.

39. Basar, E., *et al.*, "Oscillatory brain dynamics, wavelet analysis, and cognition," *Brain and Language*, Vol. 66, no. 1, pp. 146–183, 1999.

40. Von Stein, A., and Sarnthein, J., "Different frequencies for different scales of cortical integration: from local gamma to long range alpha/theta synchronization," *International Journal of Psychophysiology*, Vol. 38, no. 3, pp. 301–313, 2000.

41. Canolty, R. T., *et al.*, "High gamma power is phase-locked to theta oscillations in human neocortex," *science*, Vol. 313, no. 5793, pp. 1626–1628, 2006.

42. Murta, T., *et al.*, "Phase–amplitude coupling and the bold signal: a simultaneous intracranial eeg (iceeg)-fmri study in humans performing a finger-tapping task," *Neuroimage*, Vol. 146, pp. 438–451, 2017.

43. Salvador, R., *et al.*, "A simple view of the brain through a frequency-specific functional connectivity measure," *Neuroimage*, Vol. 39, no. 1, pp. 279–289, 2008.

44. Song, X., Zhang, Y., and Liu, Y., "Frequency specificity of regional homogeneity in the resting-state human brain," *PLoS ONE*, Vol. 9, no. 1, p. e86818, 2014.

45. Baria, A. T., *et al.*, "Anatomical and functional assemblies of brain bold oscillations," *Journal of Neuroscience*, Vol. 31, no. 21, pp. 7910–7919, 2011.

46. Buxton, R. B., *et al.*, "Modeling the hemodynamic response to brain activation," *Neuroimage*, Vol. 23, pp. S220–S233, 2004.

47. Logothetis, N. K., *et al.*, "Neurophysiological investigation of the basis of the fmri signal," *Nature*, Vol. 412, no. 6843, pp. 150–157, 2001.

48. Ritter, P., and Villringer, A., "simultaneous eeg–fmri," *Neuroscience & Biobehavioral Reviews*, Vol. 30, no. 6, pp. 823–838, 2006.

49. Rabinovich, M. I., Friston, K. J., and Varona, P., *Principles of brain dynamics*, MIT Press Cambridge, Mass, 2012.

50. Deco, G., Jirsa, V., and Friston, K. J., "The dynamical and structural basis of brain activity," 2012.

51. Cabeza, R., and Kingstone, A., *Handbook of functional neuroimaging of cognition*, Mit Press, 2006.

52. Cabeza, R., and Nyberg, L., "Imaging cognition ii: An empirical review of 275 pet and fmri studies," *Journal of Cognitive Neuroscience*, Vol. 12, no. 1, pp. 1–47, 2000.

53. Fuster, J. M., "The cognit: a network model of cortical representation," *International Journal of Psychophysiology*, Vol. 60, no. 2, pp. 125–132, 2006.

54. Friston, K. J., "Functional and effective connectivity in neuroimaging: a synthesis," *Human Brain Mapping*, Vol. 2, no. 1-2, pp. 56–78, 1994.

55. Friston, K. J., "Models of brain function in neuroimaging," *Annu. Rev. Psychol.*, Vol. 56, pp. 57–87, 2005.

56. Jirsa, V. K., and McIntosh, A. R., *Handbook of brain connectivity*, Vol. 1, Springer, 2007.

57. Avena-Koenigsberger, A., Misic, B., and Sporns, O., "Communication dynamics in complex brain networks," *Nature Reviews Neuroscience*, Vol. 19, no. 1, pp. 17–33, 2018.

58. Sporns, O., "Networks of the brain: quantitative analysis and modeling," *Analysis and Function of Large-Scale Brain Networks*, Vol. 7, pp. 7–13, 2010.

59. Bassett, D. S., and Bullmore, E. T., "Small-world brain networks revisited," *The Neuroscientist*, Vol. 23, no. 5, pp. 499–516, 2017.

60. Deco, G., *et al.*, "Rethinking segregation and integration: contributions of whole-brain modelling," *Nature Reviews Neuroscience*, Vol. 16, no. 7, pp. 430–439, 2015.

61. Shine, J. M., *et al.*, "The dynamics of functional brain networks: integrated network states during cognitive task performance," *Neuron*, Vol. 92, no. 2, pp. 544–554, 2016.

62. Van Den Heuvel, M. P., *et al.*, "Efficiency of functional brain networks and intellectual performance," *Journal of Neuroscience*, Vol. 29, no. 23, pp. 7619–7624, 2009.

63. Alavash, M., *et al.*, "Is functional integration of resting state brain networks an unspecific biomarker for working memory performance?," *Neuroimage*, Vol. 108, pp. 182–193, 2015.

64. Fransson, P., Schiffler, B. C., and Thompson, W. H., "Brain network segregation and integration during an epoch-related working memory fmri experiment," *Neuroimage*, Vol. 178, pp. 147–161, 2018.

65. Wang, R., *et al.*, "Hierarchical connectome modes and critical state jointly maximize human brain functional diversity," *Physical Review Letters*, Vol. 123, no. 3, p. 038301, 2019.

66. Lord, L.-D., *et al.*, "Understanding principles of integration and segregation using whole-brain computational connectomics: implications for neuropsychiatric disorders," *Philosophical Transactions of the Royal Society A: Mathematical, Physical and Engineering Sciences*, Vol. 375, no. 2096, p. 20160283, 2017.

67. Shine, J. M., *et al.*, "The modulation of neural gain facilitates a transition between functional segregation and integration in the brain," *Elife*, Vol. 7, p. e31130, 2018.

68. Allen, E. A., *et al.*, "Tracking whole-brain connectivity dynamics in the resting state," *Cerebral Cortex*, Vol. 24, no. 3, pp. 663–676, 2014.

69. Lurie, D. J., *et al.*, "Questions and controversies in the study of time-varying functional connectivity in resting fmri," *Network Neuroscience*, Vol. 4, no. 1, pp. 30–69, 2020.

70. Kaboodvand, N., van den Heuvel, M. P., and Fransson, P., "Adaptive frequency-based modeling of whole-brain oscillations: Predicting regional vulnerability and hazardousness rates," *Network Neuroscience*, Vol. 3, no. 4, pp. 1094–1120, 2019.

71. Broca, P., *et al.*, "Perte de la parole, ramollissement chronique et destruction partielle du lobe antérieur gauche du cerveau," *Bull Soc Anthropol*, Vol. 2, no. 1, pp. 235–238, 1861.

72. Catani, M., and Mesulam, M., "The arcuate fasciculus and the disconnection theme in language and aphasia: history and current state," *Cortex*, Vol. 44, no. 8, pp. 953–961, 2008.

73. Geschwind, N., "Disconnexion syndromes in animals and man," *Brain*, Vol. 88, no. 3, pp. 585–585, 1965.

74. Mesulam, M.-M., "Fifty years of disconnexion syndromes and the geschwind legacy," *Brain*, Vol. 138, no. 9, pp. 2791–2799, 2015.

75. Biswal, B. B., Kylen, J. V., and Hyde, J. S., "Simultaneous assessment of flow and bold signals in resting-state functional connectivity maps," *NMR in Biomedicine*, Vol. 10, no. 4-5, pp. 165–170, 1997.

76. Greicius, M. D., *et al.*, "Functional connectivity in the resting brain: a network analysis of the default mode hypothesis," *Proceedings of the National Academy of Sciences*, Vol. 100, no. 1, pp. 253–258, 2003.

77. Damoiseaux, J. S., *et al.*, "Consistent resting-state networks across healthy subjects," *Proceedings of the National Academy of Sciences*, Vol. 103, no. 37, pp. 13848–13853, 2006.

78. van den Heuvel, M. P., *et al.*, "Small-world and scale-free organization of voxel-based resting-state functional connectivity in the human brain," *Neuroimage*, Vol. 43, no. 3, pp. 528–539, 2008.

79. Greicius, M. D., *et al.*, "Persistent default-mode network connectivity during light sedation," *Human Brain Mapping*, Vol. 29, no. 7, pp. 839–847, 2008.

80. Shulman, G. L., *et al.*, "Common blood flow changes across visual tasks: I. increases in subcortical structures and cerebellum but not in nonvisual cortex," *Journal of Cognitive Neuroscience*, Vol. 9, no. 5, pp. 624–647, 1997.

81. Buckner, R. L., *et al.*, "Molecular, structural, and functional characterization of alzheimer's disease: evidence for a relationship between default activity, amyloid, and memory," *Journal of Neuroscience*, Vol. 25, no. 34, pp. 7709–7717, 2005.

82. Posner, M. I., Petersen, S. E., *et al.*, "The attention system of the human brain," *Annual Review of Neuroscience*, Vol. 13, no. 1, pp. 25–42, 1990.

83. Uddin, L. Q., Yeo, B., and Spreng, R. N., "Towards a universal taxonomy of macro-scale functional human brain networks," *Brain Topography*, Vol. 32, no. 6, pp. 926–942, 2019.

84. Dosenbach, N. U., *et al.*, "Distinct brain networks for adaptive and stable task control in humans," *Proceedings of the National Academy of Sciences*, Vol. 104, no. 26, pp. 11073–11078, 2007.

85. Seeley, W. W., *et al.*, "Dissociable intrinsic connectivity networks for salience processing and executive control," *Journal of Neuroscience*, Vol. 27, no. 9, pp. 2349–2356, 2007.

86. Sejnowski, T. J., *et al.*, "Time for a new neural code?," *Nature*, Vol. 376, no. 6535, pp. 21–22, 1995.

87. De Luca, M., *et al.*, "fmri resting state networks define distinct modes of long-distance interactions in the human brain," *Neuroimage*, Vol. 29, no. 4, pp. 1359–1367, 2006.

88. Smith, S. M., *et al.*, "Correspondence of the brain's functional architecture during activation and rest," *Proceedings of the National Academy of Sciences*, Vol. 106, no. 31, pp. 13040–13045, 2009.

89. Tamber-Rosenau, B. J., Asplund, C. L., and Marois, R., "Functional dissociation of the inferior frontal junction from the dorsal attention network in top-down attentional control," *Journal of Neurophysiology*, Vol. 120, no. 5, pp. 2498–2512, 2018.

90. Gordon, E. M., *et al.*, "Precision functional mapping of individual human brains," *Neuron*, Vol. 95, no. 4, pp. 791–807, 2017.

91. Menon, V., and Uddin, L. Q., "Saliency, switching, attention and control: a network model of insula function," *Brain Structure and Function*, Vol. 214, pp. 655–667, 2010.

92. Uddin, L. Q., *et al.*, "Structure and function of the human insula," *Journal of Clinical Neurophysiology*, Vol. 34, no. 4, pp. 300–306, 2017.

93. Dixon, M. L., *et al.*, "Heterogeneity within the frontoparietal control network and its relationship to the default and dorsal attention networks," *Proceedings of the National Academy of Sciences*, Vol. 115, no. 7, pp. E1598–E1607, 2018.

94. Murphy, A. C., *et al.*, "Multimodal network dynamics underpinning working memory," *Nature Communications*, Vol. 11, no. 1, p. 3035, 2020.

95. Spreng, R. N., "The fallacy of a âtask-negativeâ network," *Frontiers in Psychology*, Vol. 3, p. 145, 2012.

96. Zhu, S., *et al.*, "Resting state brain function analysis using concurrent bold in asl perfusion fmri," *PLoS ONE*, Vol. 8, no. 6, p. e65884, 2013.

97. Lord, L.-D., *et al.*, "Cerebral energy metabolism and the brainâs functional network architecture: an integrative review," *Journal of Cerebral Blood Flow & Metabolism*, Vol. 33, no. 9, pp. 1347–1354, 2013.

98. Engel, J., *et al.*, "Connectomics and epilepsy," *Current Opinion in Neurology*, Vol. 26, no. 2, pp. 186–194, 2013.

99. Ghuman, A. S., McDaniel, J. R., and Martin, A., "A wavelet-based method for measuring the oscillatory dynamics of resting-state functional connectivity in meg," *NeuroImage*, Vol. 56, no. 1, pp. 69–77, 2011.

100. James, W., *The Principles of Psychology*, Henry Holt, 1890.

101. Deco, G., *et al.*, "The dynamics of resting fluctuations in the brain: metastability and its dynamical cortical core," *Scientific Reports*, Vol. 7, no. 1, p. 3095, 2017.

102. Buzsáki, G., *Rhythms of the Brain*, Oxford University Press, 2006.

103. Fries, P., "A mechanism for cognitive dynamics: neuronal communication through neuronal coherence," *Trends in Cognitive Sciences*, Vol. 9, no. 10, pp. 474–480, 2005.

104. Fries, P., "Rhythms for cognition: communication through coherence," *Neuron*, Vol. 88, no. 1, pp. 220–235, 2015.

105. Womelsdorf, T., *et al.*, "Modulation of neuronal interactions through neuronal synchronization," *Science*, Vol. 316, no. 5831, pp. 1609–1612, 2007.

106. Başar, E., *et al.*, "Gamma, alpha, delta, and theta oscillations govern cognitive processes," *International Journal of Psychophysiology*, Vol. 39, no. 2-3, pp. 241–248, 2001.

107. Knyazev, G. G., "Motivation, emotion, and their inhibitory control mirrored in brain oscillations," *Neuroscience & Biobehavioral Reviews*, Vol. 31, no. 3, pp. 377–395, 2007.

108. Voytek, B., and Knight, R. T., "Dynamic network communication as a unifying neural basis for cognition, development, aging, and disease," *Biological Psychiatry*, Vol. 77, no. 12, pp. 1089–1097, 2015.

109. Steriade, M., Timofeev, I., and Grenier, F., "Natural waking and sleep states: a view from inside neocortical neurons," *Journal of Neurophysiology*, Vol. 85, no. 5, pp. 1969–1985, 2001.

110. Vanhatalo, S., *et al.*, "Infraslow oscillations modulate excitability and interictal epileptic activity in the human cortex during sleep," *Proceedings of the National Academy of Sciences*, Vol. 101, no. 14, pp. 5053–5057, 2004.

111. da Silva, F. L., "Eeg and meg: relevance to neuroscience," *Neuron*, Vol. 80, no. 5, pp. 1112–1128, 2013.

112. Goense, J. B., and Logothetis, N. K., "Neurophysiology of the bold fmri signal in awake monkeys," *Current Biology*, Vol. 18, no. 9, pp. 631–640, 2008.

113. Logothetis, N. K., "What we can do and what we cannot do with fmri," *Nature*, Vol. 453, no. 7197, pp. 869–878, 2008.

114. Laufs, H., "Endogenous brain oscillations and related networks detected by surface eegâcombined fmri," *Human Brain Mapping*, Vol. 29, no. 7, pp. 762–769, 2008.

115. Favaretto, C., *et al.*, "Multi-band meg signatures of bold connectivity reorganization during visuospatial attention," *NeuroImage*, Vol. 230, p. 117781, 2021.

116. Cordes, D., *et al.*, "Frequencies contributing to functional connectivity in the cerebral cortex in âresting-stateâ data," *American Journal of Neuroradiology*, Vol. 22, no. 7, pp. 1326–1333, 2001.

117. Greicius, M. D., *et al.*, "Functional connectivity in the resting brain: a network analysis of the default mode hypothesis," *Proceedings of the National Academy of Sciences*, Vol. 100, no. 1, pp. 253–258, 2003.

118. Wise, R. G., *et al.*, "Resting fluctuations in arterial carbon dioxide induce significant low frequency variations in bold signal," *NeuroImage*, Vol. 21, no. 4, pp. 1652–1664, 2004.

119. Birn, R. M., *et al.*, "Separating respiratory-variation-related fluctuations from neuronal-activity-related fluctuations in fmri," *NeuroImage*, Vol. 31, no. 4, pp. 1536–1548, 2006.

120. Niazy, R. K., *et al.*, "Spectral characteristics of resting state networks," *Progress in Brain Research*, Vol. 193, pp. 259–276, 2011.

121. Zuo, X.-N., *et al.*, "The oscillating brain: complex and reliable," *NeuroImage*, Vol. 49, no. 2, pp. 1432–1445, 2010.

122. Baria, A. T., *et al.*, "Anatomical and functional assemblies of brain bold oscillations," *Journal of Neuroscience*, Vol. 31, no. 21, pp. 7910–7919, 2011.

123. Kalcher, K., *et al.*, "The spectral diversity of resting-state fluctuations in the human brain," *PLoS ONE*, Vol. 9, no. 4, p. e93375, 2014.

124. Wu, C.-W., *et al.*, "Frequency specificity of functional connectivity in brain networks," *NeuroImage*, Vol. 42, no. 3, pp. 1047–1055, 2008.

125. Sasai, S., *et al.*, "Frequency-specific network topologies in the resting human brain," *Frontiers in Human Neuroscience*, Vol. 8, p. 1022, 2014.

126. Thompson, W. H., and Fransson, P., "The frequency dimension of fmri dynamic connectivity: Network connectivity, functional hubs and integration in the resting brain," *NeuroImage*, Vol. 121, pp. 227–242, 2015.

127. Park, Y. H., *et al.*, "Frequency specific contribution of intrinsic connectivity networks to the integration in brain networks," *Scientific Reports*, Vol. 9, no. 1, p. 4072, 2019.

128. De Domenico, M., *et al.*, "Structural reducibility of multilayer networks," *Nature Communications*, Vol. 6, no. 1, p. 6864, 2015.

129. Glasser, M. F., *et al.*, "A multi-modal parcellation of human cerebral cortex," *Nature*, Vol. 536, pp. 171–178, 2016.

130. Huntenburg, J. M., *et al.*, "A systematic relationship between functional connectivity and intracortical myelin in the human cerebral cortex," *Cerebral Cortex*, Vol. 27, pp. 981–997, 2017.

131. Murray, J. D., *et al.*, "A hierarchy of intrinsic timescales across primate cortex," *Nature Neuroscience*, Vol. 17, no. 12, pp. 1661–1663, 2014.

132. Raut, R. V., *et al.*, "Organization of propagated intrinsic brain activity in individual humans," *Cerebral Cortex*, Vol. 30, pp. 1716–1734, 2020.

133. Ito, T., *et al.*, "Discovering the computational relevance of brain network organization," *Trends in Cognitive Sciences*, Vol. 24, no. 1, pp. 25–38, 2020.

134. Zaytsev, E., "'s problem of konigsberg bridges and leibniz'geometria situs," *International Archives of the History of Science*, Vol. 58, no. 160, p. 151, 2008.

135. Albert, R., and Barabási, A.-L., "Statistical mechanics of complex networks," *Reviews of Modern Physics*, Vol. 74, no. 1, pp. 47–97, 2002.

136. Newman, M. E. J., "The structure and function of complex networks," *SIAM Review*, Vol. 45, no. 2, pp. 167–256, 2003.

137. Boccaletti, S., *et al.*, "Complex networks: Structure and dynamics," *Physics Reports*, Vol. 424, pp. 175–308, 2006.

138. Eickhoff, S. B., Yeo, B. T. T., and Genon, S., "Imaging-based parcellations of the human brain," *Nature Reviews Neuroscience*, Vol. 19, no. 11, pp. 672–686, 2018.

139. Mohanty, R., *et al.*, "Rethinking measures of functional connectivity via feature extraction," *Scientific Reports*, Vol. 10, no. 1, p. 1298, 2020.

140. Peng, L., *et al.*, "Measuring functional connectivity in frequencyâdomain helps to better characterize brain function," *Human Brain Mapping*, Vol. 45, no. 10, p. e26726, 2024.

141. Simon, H. A., "The architecture of complexity," *Proceedings of the American Philosophical Society*, Vol. 106, pp. 467–482, 1962.

142. Sternberg, S., "Modular processes in mind and brain," *Cognitive Neuropsychology*, Vol. 28, no. 3-4, pp. 156–208, 2011.

143. Fortunato, S., "Community detection in graphs," *Physics Reports*, Vol. 486, no. 3-5, pp. 75–174, 2010.

144. Latora, V., and Marchiori, M., "Efficient behavior of small-world networks," *Physical Review Letters*, Vol. 87, no. 19, p. 198701, 2001.

145. Newman, M. E. J., and Girvan, M., "Finding and evaluating community structure in networks," *Physical Review E*, Vol. 69, no. 2, p. 026113, 2004.

146. Newman, M. E. J., Strogatz, S. H., and Watts, D. J., "Random graphs with arbitrary degree distributions and their applications," *Physical Review E*, Vol. 64, no. 2, p. 026118, 2001.

147. Blondel, V. D., *et al.*, "Fast unfolding of communities in large networks," *Journal of Statistical Mechanics: Theory and Experiment*, Vol. 2008, no. 10, p. P10008, 2008.

148. GuimerÃ , R., and Amaral, L. A. N., "Cartography of complex networks: modules and universal roles," *Journal of Statistical Mechanics: Theory and Experiment*, Vol. 2005, no. 02, p. P02001, 2005.

149. Power, J. D., *et al.*, "Evidence for hubs in human functional brain networks," *Neuron*, Vol. 79, no. 4, pp. 798–813, 2013.

150. Bertolero, M. A., *et al.*, "A mechanistic model of connector hubs, modularity and cognition," *Nature Human Behaviour*, Vol. 2, no. 10, pp. 765–777, 2018.

151. Bertolero, M. A., Yeo, B. T. T., and DâEsposito, M., "The modular and integrative functional architecture of the human brain," *Proceedings of the National Academy of Sciences*, Vol. 112, no. 49, pp. E6798–E6807, 2015.

152. Gratton, C., *et al.*, "Evidence for two independent factors that modify brain networks to meet task goals," *Cell Reports*, Vol. 17, no. 5, pp. 1276–1288, 2016.

153. Cole, M. W., *et al.*, "Multi-task connectivity reveals flexible hubs for adaptive task control," *Nature Neuroscience*, Vol. 16, no. 9, pp. 1348–1355, 2013.

154. Bassett, D. S., *et al.*, "Dynamic reconfiguration of human brain networks during learning," *Proceedings of the National Academy of Sciences*, Vol. 108, no. 18, pp. 7641–7646, 2011.

155. Van Essen, D. C., *et al.*, "The wu-minn human connectome project: an overview," *NeuroImage*, Vol. 80, pp. 62–79, 2013.

156. Burgess, G. C., *et al.*, "Evaluation of denoising strategies to address motion-correlated artifacts in resting-state functional magnetic resonance imaging data from the human connectome project," *Brain Connectivity*, Vol. 6, no. 9, pp. 669–680, 2016.

157. Siegel, J. S., *et al.*, "Data quality influences observed links between functional connectivity and behavior," *Cerebral Cortex*, Vol. 27, no. 9, pp. 4492–4502, 2017.

158. Kong, R., *et al.*, "Spatial topography of individual-specific cortical networks predicts human cognition, personality, and emotion," *Cerebral Cortex*, Vol. 29, no. 6, pp. 2533–2551, 2019.

159. Li, J., *et al.*, "Global signal regression strengthens association between resting-state functional connectivity and behavior," *NeuroImage*, Vol. 196, pp. 126–141, 2019.

160. Whitfield-Gabrieli, S., and Nieto-Castanon, A., "Conn: a functional connectivity toolbox for correlated and anticorrelated brain networks," *Brain Connectivity*, Vol. 2, no. 3, pp. 125–141, 2012.

161. Power, J. D., *et al.*, "Methods to detect, characterize, and remove motion artifact in resting state fmri," *NeuroImage*, Vol. 84, pp. 320–341, 2014.

162. Behzadi, Y., *et al.*, "A component based noise correction method (compcor) for bold and perfusion based fmri," *NeuroImage*, Vol. 37, no. 1, pp. 90–101, 2007.

163. Liu, T. T., Nalci, A., and Falahpour, M., "The global signal in fmri: Nuisance or information?," *NeuroImage*, Vol. 150, pp. 213–229, 2017.

164. Muschelli, J., *et al.*, "Reduction of motion-related artifacts in resting state fmri using acompcor," *NeuroImage*, Vol. 96, pp. 22–35, 2014.

165. Vinck, M., *et al.*, "The pairwise phase consistency: a bias-free measure of rhythmic neuronal synchronization," *NeuroImage*, Vol. 51, no. 1, pp. 112–122, 2010.

166. Aydore, S., Pantazis, D., and Leahy, R. M., "A note on the phase locking value and its properties," *NeuroImage*, Vol. 74, pp. 231–244, 2013.

167. Bordier, C., Nicolini, C., and Bifone, A., "Graph analysis and modularity of brain functional connectivity networks: searching for the optimal threshold," *Frontiers in Neuroscience*, Vol. 11, p. 441, 2017.

168. Achard, S., and Bullmore, E., "Efficiency and cost of economical brain functional networks," *PLoS Computational Biology*, Vol. 3, no. 2, p. e17, 2007.

169. Lynall, M. E., *et al.*, "Functional connectivity and brain networks in schizophrenia," *Journal of Neuroscience*, Vol. 30, no. 28, pp. 9477–9487, 2010.

170. Gallos, L., Sigman, M., and Makse, H. A., "The conundrum of functional brain networks: small-world efficiency or fractal modularity," *Frontiers in Physiology*, Vol. 3, p. 25745, 2012.

171. Maslov, S., and Sneppen, K., "Specificity and stability in topology of protein networks," *Science*, Vol. 296, no. 5569, pp. 910–913, 2002.

172. Humphries, M. D., Gurney, K., and Prescott, T. J., "The brainstem reticular formation is a small-world, not scale-free, network," *Proceedings of the Royal Society B: Biological Sciences*, Vol. 273, no. 1585, pp. 503–511, 2006.

173. Nicolini, C., *et al.*, "Scale-resolved analysis of brain functional connectivity networks with spectral entropy," *NeuroImage*, Vol. 211, p. 116603, 2020.

174. Leiserson, C. E., *et al.*, *Introduction to Algorithms*, Vol. 3, Cambridge, MA, USA: MIT Press, 1994.

175. Fenn, D. J., *et al.*, "Dynamic communities in multichannel data: An application to the foreign exchange market during the 2007â2008 credit crisis," *Chaos: An Interdisciplinary Journal of Nonlinear Science*, Vol. 19, no. 3, p. 033119, 2009.

176. Klimm, F., *et al.*, "Individual node's contribution to the mesoscale of complex networks," *New Journal of Physics*, Vol. 16, no. 12, p. 125006, 2014.

177. Pedersen, M., *et al.*, "Reducing the influence of intramodular connectivity in participation coefficient," *Network Neuroscience*, Vol. 4, no. 2, pp. 416–431, 2020.

178. Barch, D. M., *et al.*, "Function in the human connectome: task-fmri and individual differences in behavior," *NeuroImage*, Vol. 80, pp. 169–189, 2013.

179. Penttonen, M., and Buzsáki, G., "Natural logarithmic relationship between brain oscillators," *Thalamus & Related Systems*, Vol. 2, no. 2, pp. 145–152, 2003.

180. Bayram, A., *et al.*, "Achromatic temporal-frequency responses of human lateral geniculate nucleus and primary visual cortex," *Vision Research*, Vol. 127, pp. 177–185, 2016.

181. Moussa, M. N., *et al.*, "Consistency of network modules in resting-state fmri connectome data," *PLoS ONE*, Vol. 7, no. 8, p. e44428, 2012.

182. Doucet, G., *et al.*, "Brain activity at rest: a multiscale hierarchical functional organization," *Journal of Neurophysiology*, Vol. 105, no. 6, pp. 2753–2763, 2011.

183. Gravel, N., *et al.*, "Phase-synchronization-based parcellation of resting state fmri signals reveals topographically organized clusters in early visual cortex," *NeuroImage*, Vol. 170, pp. 424–433, 2018.

184. Keller, C. J., *et al.*, "Neurophysiological investigation of spontaneous correlated and anticorrelated fluctuations of the bold signal," *Journal of Neuroscience*, Vol. 33, no. 15, pp. 6333–6342, 2013.

185. Yaesoubi, M., *et al.*, "Frequency-aware summarization of resting-state fmri data," *Frontiers in Systems Neuroscience*, Vol. 14, p. 16, 2020.

186. Ries, A., *et al.*, "Grading of frequency spectral centroid across resting-state networks," *Frontiers in Human Neuroscience*, Vol. 12, p. 436, 2018.

187. Ma, J., *et al.*, "Integrated and segregated frequency architecture of the human brain network," *Brain Structure and Function*, Vol. 226, pp. 335–350, 2021.

188. Von Stein, A., and Sarnthein, J., "Different frequencies for different scales of cortical integration: from local gamma to long range alpha/theta synchronization," *International Journal of Psychophysiology*, Vol. 38, no. 3, pp. 301–313, 2000.